Tampere University

FARID KHOSRAVI

POSITIONING OF THE WHEEL LOADER BY ULTRA WIDEBAND TECHNOLOGY

Faculty of Engineering and
Natural Sciences
Master of Science thesis
September 2019

ABSTRACT

FARID KHOSRAVI: POSITIONING OF THE WHEEL LOADER BY ULTRA WIDEBAND TECHNOLOGY
Master of Science thesis
Tampere University
Master's Degree Programme in Factory Automation and Industrial Informatics
September 2019

Localization is one of the most interesting fields in robotics and it can be categorized based on the environment as indoor and outdoor localization. There are several reliable solutions provided for outdoor positioning the most popular of which is the Global Navigation Satellite System (GNSS). In this regard, employing GNSS would not be a reliable method for localization inside buildings or closed environments due the absence of sufficient number of satellite signal indoors. Thus, for implementing indoor localization there are a variety of solutions proposed which can be broadly classified into two main categories. The first is localization algorithms based on wireless technologies such as Bluetooth, Wi-Fi and Global System for Mobile Communications (GSM) [1, p. 126,128]. Hardware associated with these technologies are frequently found installed with positioning not being their primary use-case. Such approaches has its own pros and cons and in order to have a more accurate localization [1, p. 127], purpose-built sensors and devices are required. The second method is concerned with employing specific technologies such as ZigBee, Radio Frequency Identification (RFID), Infrared, Ultrasonic and Ultra-Wideband technologies [2], [3] to implement the indoor localization.

In this study, in order to overcome the limitations of the GNSS system in diverse environments we employ a comprehensive system to cover both indoor and outdoor positioning of a mobile vehicle to obtain a stable and continuous localization. The mobile vehicle used for this study is an experimental wheel loader of Tampere University. When the wheel loader is outdoors, the localization follows GNSS until it enters a hall or any closed environment after which it begins to loose positioning accuracy. This study addresses this problem (loss in positioning accuracy) with Ultra-Wideband (UWB) technology that has characteristics such as high accuracy and low power consumption [4]. UWB is a multi-functional technology and is employed in various applications such as data transmission and radar. However, in this research its positioning application is surveyed. The UWB technology is employed as a complementary sensor to the GNSS, enabling indoor localization. What follows next is a brief description of the test area where the experiments are carried out and the experimental machine that is chosen as the mobile vehicle.

The test area is approximately 4000 m^2 with a combination of an open space with a tangible difference in the ground elevation between two parts and a hall in the middle with a flat ground. The hall is used as parking area for the heavy machines and in this study, it acts as an indoor environment to disturb the regular performance of the GNSS. Therefore, this leads the localization algorithm to switch from making use of GNSS data to UWB data. The experimental wheel loader of Tampere University is equipped with heterogeneous devices and sensors such as Novatron RTK-GNSS, UWB mobile node and one Simulink Real-time PC. This real time PC is connected to the local Wi-Fi network to transfer the recorded data and is responsible for storing and executing the localization model and recording real-time data.

Further, in this thesis, we study two possible methods to enhance the localization accuracy which are based on the Trilateration and the Extended Kalman Filter algorithm. In our experiments, we observed that the best positioning result is achieved via employing the Trilateration method to estimate the initial point and then subsequently tracking the mobile machine using Extended Kalman Filter on the range data. As a result, we achieved near similar results to the GNSS data in indoor environments in our work.

Keywords: Ultra-Wideband, UWB, indoor localization, Extended Kalman Filter, EKF and Trilateration.

PREFACE

This thesis was done as a part of DIMECC's D4V project regarding capability of Ultra Wide-band in localization through Faculty of Engineering and Natural Sciences, Automation Technology and Mechanical Engineering unit – Innovative Hydraulics and Automation at Tampere University – Hervanta Campus.

Firstly, I would like to thank my supervisor Professor Reza Ghabcheloo for valuable discussions on the subject. Moreover, I would express my gratitude and thankfulness to my other supervisor Mika Hyvönen for the positive feedbacks and effective experimental hints. Thanks are also extended to all my friends who support me during the work especially Jonathan Shabulinzenze and Mostafa Mansour. Finally, I should express my special thankfulness and appreciation to my father, mother and sister who always support me in all stages of my life.

Tampere, 23 September 2019

Farid Khosravi

CONTENTS

LIST OF FIGURES

LIST OF SYMBOLS AND ABBREVIATIONS

ACC	Automatic Congestion Control
ALOHA	Additive Links On-line Hawaii Area
AoA	Angle of Arrival
CAN	Controller Area Network
CDMA	Code Division Multiple Access
CRE	Coarse Range Estimate
EKF	Extended Kalman Filter
FRE	Filtered Range Estimate
FRV	Filtered Range Velocity
GNSS	Global Navigation Satellite System
GPS	Global Positioning System
GSM	Groupe Spécial Mobile
Hz	Hertz
IDE	Integrated Development Environment
IMU	Inertial Measurement Unit
LOS	Line Of Sight
LSE	Least Square Estimation
MAC	Medium Access Control
ms	millisecond
NLOS	Non-Line Of Sight
PF	Particle Filter
PII	Pulse Integration Index
PRM	Precision Range Measurement
RFID	Radio Frequency Identification
RSSI	Received Signal Strength Indicator
RTK	Real-Time Kinematic
RTT	Round Trip Time
SDS-TWR	Symmetric Double-Sided Two-Way Ranging
SMA	SubMiniature version A
SNR	Signal to Noise Ratio
SPI	Serial Peripheral Interface
TDMA	Time Division Multiple Access
TDoA	Time Difference of Arrival
ToA	Time of Arrival
ToF	Time of Flight
TWR	Two-Way Ranging
TW-ToF	Two-Way Time of Flight
UML	Unified Modeling Language
UWB	Ultra-Wideband
WSN	Wireless Sensor Network

1. INTRODUCTION

This chapter provides a presentation to this study. Firstly, a short background about localization and UWB, followed by problem definition and objective and finally thesis outline is mentioned as the last section.

1.1 Background

UWB is a radio-based technology extensively applied in communication aims while it has other considerable applications in the range measurement and positioning which is also an interesting field in various industries and radar technologies. Localization in the word means the process of constraining something to a specific place[5] yet it has a more particular definition in robotics: estimating the coordinates of a robot based on the external information and a map of the environment is called localization on robotics [6, p. 3]. Obviously, technologies like cell phones, warehouse management, autonomous vehicles are extremely interested to apply and integrate the latest and the most accurate methods and devices of localization to their products.

With the purpose of implementing a robust and relatively accurate localization system, at first, the localization environment should be specified. For instance, if the purpose is to estimate the location of a specific target object in an open space(outdoor), this purpose will be attained by applying a device which is equipped by a Global Navigation Satellite System (GNSS) component such as Global Positioning System (GPS)[7] like a cell phone and then the estimated location will be gained in the world map. However, a number of definite restrictions regarding application of GPS exist where there is no Line Of Sight (LOS) between the GPS device and at least four navigation satellites during measurement process[8, p. 2]. According to this restriction, GPS is not an inappropriate choice for Indoor positioning as well. This limitation led the researchers to propose several solutions in indoor positioning.

The main problem appears when the localization of an entity via GNSS within a building or a closed environment which does not have LOS to at least 4 navigation satellites is required. This case is called Indoor Localization and there are several solutions regarding it which are classified into two main types. The first one is applying on the hardware infrastructure and devices which are installed for other applications like as Wi-Fi, Global System for Mobile Communications (GSM) and Bluetooth devices[1, p. 126,128]. Though there are some restrictions on the utilization of these methods as well. As an example, Bluetooth is just appropriate for short-range positioning due to its maximum range which is 20 to 30 meters[9, p. 2]; moreover, the localization accuracy of Global System for Mobile communications (GSM) is highly affected by buildings and floors and has a tolerance of 2.5 meters [2, p. 3]. The second method requires specific hardware and devices for localization. Frequently, this type consists of a kind of Wireless Sensor Networks (WSN) such as ZigBee, RFID, Infrared, Ultrasonic and Ultra-Wide Band (UWB)[3][2] which are able to provide a signal factor called Received Signal Strength Indicator (RSSI)[3] that helps us to determine whether the measurement is valid or not. Each of these technologies has its own advantages and disadvantages which can be studied more in details [2], [3], [10], [11].

One of the relatively accurate indoor positioning systems in WSNs is Ultra-Wideband (UWB) technology[4]. UWB localization systems use a radio frequency technology gaining the greatest possible bandwidth that is more than 500 MHz over a few Gigahertz at the lowest main frequency and is able to achieve relative bandwidth of 25 to 100%[12]. This technology can be applied in various fields such as communication, radar, range measurement and localization[13]. Additionally, it is immune to interferences with other radio waves due to the wideband feature.

1.2 Problem Definition

Indoor positioning has plenty of applications in real-life scenarios such as positioning cars in parking lots, finding a book in a smart large library or locating a specific product in a warehouse. In this thesis, continues positioning is implemented by means of GNSS and UWB devices in a way that where GNSS fails, UWB proceeds the localization.

In real-time indoor and outdoor localization through different types of sensors, various issues can appear. Decision making with regard to opting the location data of the UWB device or the range data in order to implement the localization is a primary issue. The next matter is the calibration method of the UWB devices network to collate UWB localization with GNSS localization. Moreover, electing a reliable localization and tracking algorithm for UWB device should be considered. Furthermore, as UWB localization is supposed to be employed where the GNSS localization fails, the problem of synchronization appears. Detecting GNSS failure in localization, smooth switching to UWB localization and returning to the GNSS localization after having a stable localization with GNSS is another issue. Managing the NLOS range measurements despite of UWB device capability in eliminating NLOS range measurements; however, it confirms a few NLOS measurements that lead to inaccuracy in positioning. Another challenge is choosing a proper tool to support all requirements of real-time algorithm implementation.

1.3 Objective

This study is focused on the continuous localization of the Experimental wheel loader of Tampere University via GNSS and whenever GNSS fails, the localization proceeds on UWB device.

In order to achieve this target and according to the aforementioned problems a real-time model should be designed to support the following targets:

- Calculating the pose of the experimental wheel loader of Tampere University by means of a geometric method such as trilateration to find the initial point and employ the pose data in other algorithms.
- Proceeding the localization and tracking the mobile machine by applying EKF.
- Eliminating the effects of the incorrect measurements which have the temporal or spatial variation [14] that cause to have a smooth positioning.
- Monitoring the GNSS localization to detect the inaccuracy and immediately replacing it with the UWB localization.
- Keeping the wheel loader localization stable and smooth by means of intact switching between GNSS and UWB localization and vice versa.

1.4 Thesis Outline

The thesis contains 5 chapters. The first one consists of an introduction to background, problem definition and objective of this study. The second chapter comprises of the theoretical background of the UWB technology, various methods of the range measurement and networking, specifications and characteristics of the UWB device and theorem of localization methods which are related to the scope of this thesis. The next chapter is dedicated to the methodology. The fourth chapter illustrates localization execution, the results and environment analysis and the final chapter is allocated to the conclusion of this study.

2. THEORETICAL BACKGROUND

This chapter presents background on Ultra-Wideband technology, further diverse applications and various methods of range measurement via this technology, a description on the specification of the examined UWB device (P440) in this research and a couple of localization methods which are related to the scope of this thesis.

2.1 Ultra-wideband technology

Ultra-wideband (UWB) is known as a wireless communication technology that allows the transmission of data over a large bandwidth further than 500 MHz with a central frequency in the range of 3.1 to 10.6 GHz. In 2002, the Federal Communication Commission (FCC) authorized the application of unlicensed UWB for any real and legal person[15]. Since this authorization has been granted, the application of this frequency bandwidth has increased in a wide variety of fields, such as radar, indoor and outdoor positioning, imaging and data communication[10].

2.1.1 Range Measurement Techniques

Farid and Nordin et al.[11, Ch. 3] classified the wireless indoor localization methods into three main categories based on the positioning techniques used to locate an object. Their classification is presented in Figure 1. These are Proximity detection, Triangulation, and Scene Analysis. However, in the case of UWB, triangulation is the most commonly used method.

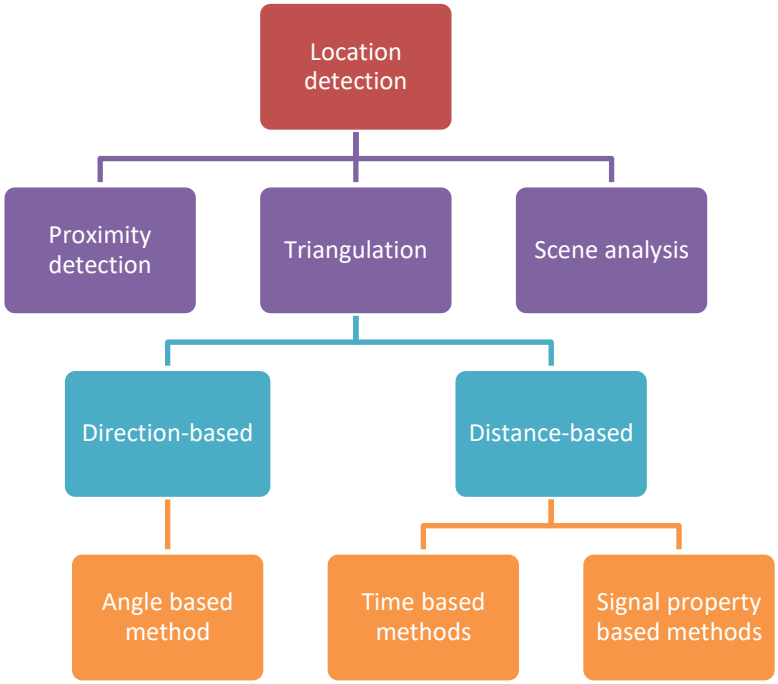

Figure 1. *Classification of Wireless Localization Techniques* [11, Fig. 3]

Triangulation is classified into two methods: direction-based and distance-based. The direction-based method involves applying angle-based measurements while the distance-based method relies on time-based measurements. The signal property-based method as can be seen in the classification diagram in Figure 1, should be considered for the radio signals and it is based on the Received Signal Strength(RSS) which is gained from the properties of the received signal on the mobile node form reference nodes[11, p. 3,4]. The mobile node is a UWB device which has the capability of movement and further it should be localized. Reference node is UWB device as well which is installed in a certain place and responses to the range request of the mobile node. It is also called Anchor.

In case of positioning and tracking algorithms via UWB, there are four categories [4, p. 1]:

1. Geometry-based
2. Bayesian techniques
3. Cost function minimization
4. Fingerprint

In this study, concentration of our discussion is on the geometry-based and Bayesian techniques methods that are both distance-based. In the following, a short description of the other methods of location detection is presented.

In this regard, proximity detection is the simplest method. It relies on the location of the nearest Anchor and the strength of the signal to find the location of the mobile node [11, p. 3]. Trilateration is a sub-method of distance-based and time-based methods which finds the mobile devices' location by applying the geometric information from at least three Anchors and the distance of the mobile node from each of them. The next one is the scene analysis method which is also called fingerprinting method. It builds a database by collecting the data of the scenes in all the locations of the intended areas and then localizes the target object in the aforementioned area based on comparing the real-time measurement of the object's closed location features with the database. Angulation or Angle of Arrival (AOA) is another method which is based on the direction of the mobile node. AOA specifies the location of the mobile node by detecting the angles between the mobile node and at least 2 reference nodes for 2-dimensional localization[11, Ch. 3]. These methods are illustrated in Figure 2.

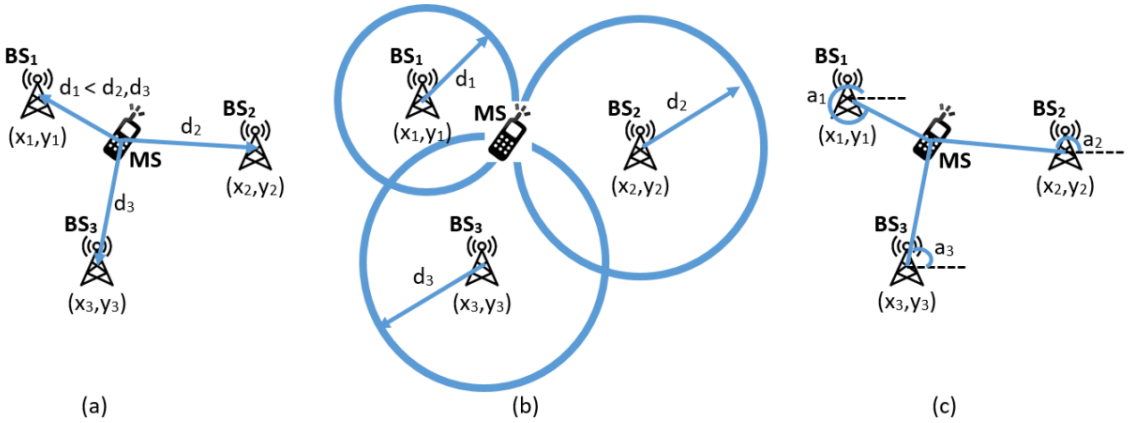

Figure 2. *Localization techniques a) Proximity, b) Trilateration, c) Angulation* [16, Fig. 1]

Time-based techniques compute the distance or range between the mobile node and each reference based on the time difference of sending and receiving the signal between mobile and reference nodes. A number of time-based techniques to calculate the range between the mobile node and reference node such as [11, Ch. 3][17, p. 15]:

1. Time of Arrival (ToA) or Time of Flight (ToF)
2. Time Difference of Arrival (TDoA)
3. Two-Way Ranging (TWR) or Two-Way Time of Flight (TW-ToF)
4. Symmetric Double-Sided Two-Way Ranging (SDS-TWR)

Time of Arrival

This method of distance measurement is based on the precise synchronization of the arrival time of the signal from the mobile node to each anchor and then the returning time of the signal from the relative anchor to the mobile node. The time that each sensor takes to process and transmit the data is known; therefore, the signal floating time between the mobile and the anchor node can be calculated by subtracting the sent time from the mobile node and the time of arrival of the signal to the anchor. The distance between the mobile and anchor node can be calculated by multiplying this time with the speed of the signal in the environment.

The high dependency on synchronization of sender and receiver nodes is the most important challenge of this method. For instance, a 3 nanoseconds difference in synchronization can lead to almost 1-meter error in distance measurement[18, p. 1]. Due to this problem, it is vital that all the anchors require to be accurately synchronized with the mobile node. Actually, this is the main drawback of this method as small errors in the initial synchronization can cause large errors in the measurements[11, p. 3,4].

Time Difference of Arrival

This technique involves measuring the distance among a number of references with certain coordinates and employs relative time measurements at the arrival nodes according to their position in the total time measurements. This method does not need synchronization of the time resource to be able to resolve the location of the mobile node. In this way, a transmission with an unknown starting time is received in different reception units so that only the receiver nodes need to be synchronized rather than all the anchors. The difference in the arrival time measurements generates a variety of hyperbolic curves and the intersection point of such curves is the actual location of the mobile node. The localization employs TDoA, is called multilateration[11, p. 4].

Two-Way Ranging

This method is the most popular method of range measurement in radio frequency range measurement methods due to the elimination of the synchronization problem[17, p. 15]. The calculation of ToA is based on the synchronization

between two nodes (Mobile node is Device A and reference node is Device B), but the difference between this method and ToA is in the number of clocks which are used. ToA has 2 clocks in both end nodes while Two-Way Ranging (TWR) has just 1 clock in the Device A. TWR technique is represented in Figure 3[18]. t_{replyB} denotes response time of Device B to the request of Device A and it completely dependent on the device hardware characteristics and t_{replyA} denotes the same regard Device A to Device B. t_{round} means the total time of the sending and receiving the signal between Device A and Device B. t_p represents the ToA and can be calculated by the equation (1) assuming that there is no clock drift[18, p. 1].

$$t_p = \frac{1}{2}(t_{round} - t_{replyB}) \tag{1}$$

TWR only eliminates the errors that might happen due to the faulty synchronization between devices, yet it still suffers from another type of error. This error belongs to the crystal of the oscillator which generates the clocks and is called offset of the oscillator. Crystal offset of the oscillator is produced when the crystal drifts from the reference time. By considering the crystal offsets of Device A and B (e_A and e_B) the estimated ToA ($\hat{t}_p$) can be calculated via equation 2[18, p. 2].

$$\hat{t}_p = \frac{1}{2}\Big(t_{round}(1 + e_A) - t_{replyB}(1 + e_B)\Big) \tag{2}$$

$$\hat{t}_p - t_p = \frac{1}{2}\Big(2t_p e_A + t_{replyB}(e_A - e_B)\Big) \tag{3}$$

The error is calculated by subtracting equation (1) from (2) and is shown in equation (3)[18, p. 2].

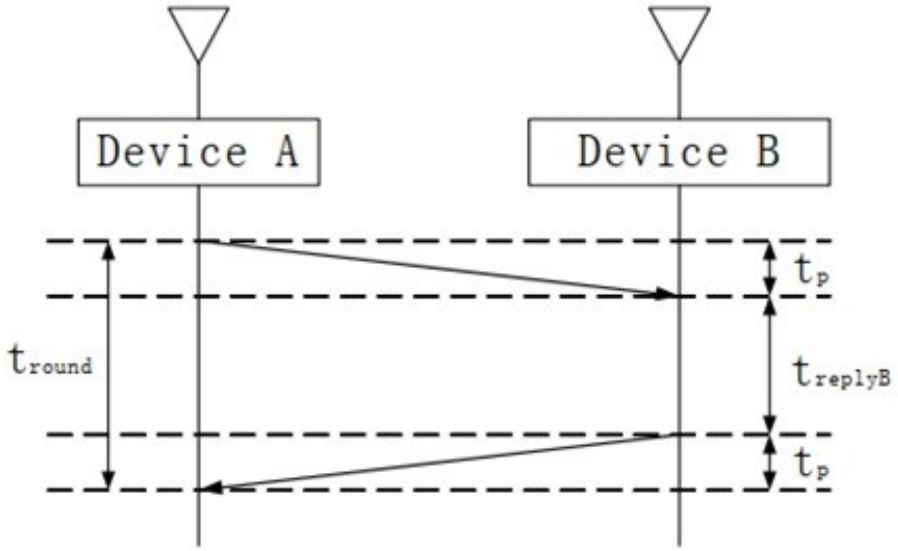

Figure 3. *Two-Way Ranging*[18, Fig. 1]

Generally, the value of the t_p is much smaller than t_{replyB} thus the error of the oscillator offset is represented by equation 4[18, p. 2].

$$\hat{t}_p - t_p = \frac{1}{2} t_{replyB}(e_A - e_B) \tag{4}$$

Two-Way Ranging is also called Two-Way Time of Flight (TW-TOF)[19] and Round Trip Time (RTT)[11, p. 4]. The range measurement method of the P440 is Two-Way Time of Flight (TW-TOF).

Symmetric Double-Sided Two-Way Ranging (SDS-TWR)

This method is applied by IEEE 802.15.4a[19] In order to decrease the crystal offset of the TWR. To achieve this goal, another transmission of the ranging message is added to the process of the TWR. After one transmission of the ranging message, Device A waits for a while (t_{replyA}, its value depends on the hardware characteristics of the Device A, such as t_{replyB}) and then sends another ranging message to the Device B. After receiving the signal, device B will mark its time. The process of the SDS-TWR is shown in Figure 4. The equations of the 2 round transmission of the signal are (5) and (6)[18, p. 2,3],[19]:

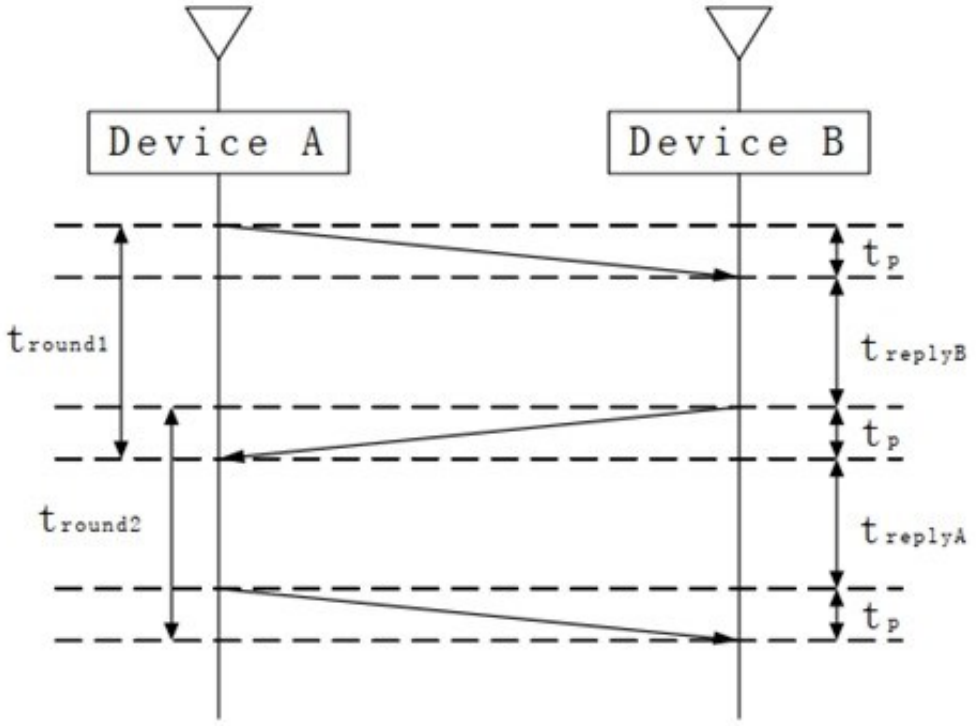

Figure 4. *Symmetric Double-Sided Two-Way Ranging*[18, Fig. 4]

$$t_{round1} = 2t_p + t_{replyB} \tag{5}$$

$$t_{round2} = 2t_p + t_{replyA} \tag{6}$$

According to the whole procedure of the signal transmission, the following equations, (7) and (8), are obtained to calculate t_p that is ToF:

$$t_{round1} + t_{round2} = 4t_p + t_{replyB} + t_{replyA} \tag{7}$$

$$t_p = \frac{1}{4}\Big(\big(t_{round1} - t_{replyA}\big) + \big(t_{round2} - t_{replyB}\big)\Big) \tag{8}$$

In order to calculate the crystal offset, first, the ToF estimation should be calculated in equation (9) and then in the equations (10) and (11) the value of the crystal offset is computed:

$$\hat{t}_p = \frac{1}{4}\Big(\big(t_{round1} - t_{replyA}\big)(1 + e_A) + \big(t_{round2} - t_{replyB}\big)(1 + e_B)\Big) \tag{9}$$

$$\hat{t}_p - t_p = \frac{1}{2}t_p(e_A - e_B) + \frac{1}{4}\Big(\big(t_{replyB} - t_{replyA}\big)(e_A - e_B)\Big) \tag{10}$$

t_p has an Insignificant value in comparison with $t_{replyB} - t_{replyA}$, moreover equation (10) can be simplified to equation (11) and the crystal offset would be gained via subtracting $\hat{t}_p$ and t_p [18, p. 2], [19, p. 126]:

$$\hat{t}_p - t_p = \frac{1}{4}\Big(\big(t_{replyB} - t_{replyA}\big)(e_A - e_B)\Big) \tag{11}$$

2.1.2 Radar systems

Ultra-Wideband technology is capable of being employed in radar systems because of its characteristics. Due to its short pulses feature, UWB obtains a perfect range resolution and also a high precision distance. In the radar application, UWB performs relatively accurate in detecting the objects which are very close to each other based on its wide bandwidth. Even in the high loss signal environments such as stairs, walls and buildings, it retains the high performance in detection. This technology is also immune against interferences such as various weather conditions or other radio frequency signals due to its CDMA feature[20]. Via partaking a well-designed antenna, UWB can cover angular resolution as well as range resolution.

An application of the UWB in radar systems is in the vehicle industry; however, the frequency range is between 22 and 29 GHz and also is equipped by a directional antenna under UWB rules in different types of cars. By applying this technology, the performance of some smart cars' features such as collision avoidance, air-bag activation and suspension system will slightly improve[21, p. 199].

2.1.3 Communication systems

The other application of the UWB technology is in the communication systems due to its capability in transmitting data by its large bandwidth. The extraordinarily wide bandwidth is applied as the backbone of a wireless local area network with having 1-gigabit data rates per second. Based on the UWB feature, there is less fading related to the material of the buildings in comparison with high-frequency bandwidth methods. When the UWB operates in a lower frequency, both path losing along with emitting power decline and the system presents a better performance[22].

Building a network of sensors is another application of the UWB as a communication link. This could release the sensor networks from the problem of wiring and its expenses. For example, in medical fields, when sensors are connected to the body of the patient, there is no limitation in the movement of the patient due to the sensor's wiring and it also transfers the needed data to the machines. Moreover, not only UWB transmits the data, but also it can function as a sensor such as a heartbeat or respiration sensor and even in some cases as medical imaging[22].

In order to obtain a network with several users, UWB pulses play the main role in creating a very high data rate with high performance. UWB waveforms are reasonably protected against the effects of the multipath interferences as observed in indoor environments and mobile applications. In addition, due to the exceptionally short waveforms, packet structure and also Time Division Multiple Access (TDMA) protocols are willingly performed to support communications in a network with multiple users [22].

In order to implement a flawless wireless sensor network of UWB devices, it is required to obtain the network based on the Medium Access Control (MAC) protocols to organize access to the communication channel among network devices when each of them has data to transmit. MAC consists of several protocols such as Additive Links On-line Hawaii Area (ALOHA)[23, p. 159], Time Division Multiple Access (TDMA), Code Division Multiple Access (CDMA) and etc.[24, p. 2]. The ALOHA, TDMA and CDMA protocols are described in the following since they are needed to be known in the next chapters.

Additive Links On-line Hawaii Area (ALOHA)

In 1968, the scientists of the University of Hawaii commenced working on a computer-computer or console-computer communication method which was led to developing Additive Links On-line Hawaii Area (ALOHA) protocol [25, p. 1]. ALOHA is a random access protocol which coordinates network devices access to a communication network channel [24, p. 2]. In this protocol, each device transmits its data frame whenever desires to transmit with no network manager framework or time slot in order to prevent collision among data frames from various network members. Then the device times out to receive the acknowledgment. In

case, the acknowledgment is not received, the data frame assumes to be lost due to the collision with the data frame of another device and the device after waiting a random time retransmits it[26, p. 28]. ALOHA is an appropriate protocol for small networks with a few numbers of devices due to the low probability of interference among devices[19, p. 7]. By applying the acknowledgment method and retransmission of collided data frames ALOHA partially covers the collision problem. Slotted ALOHA is the next generation of the ALOHA and the performance improved two times in comparison with ALOHA[27, p. 4]. In this protocol, the time interval is divided into discrete slots and each slot is dedicated only to the time duration of one frame. The devices need to begin the data frames transmission at the beginning of each time slot[26, p. 42].

Time Division Multiple Access (TDMA)

Time Division Multiple Access is a communication protocol and allows multiple users to access a communication channel by the division of the time into several non-overlapping time slots. Each time slot is allocated to a specific user and the users transmit their data packets in a sequential order rapidly by using their own time slots. Thus there is only one active transmission at each moment[28]. This feature makes it possible to use a radio frequency channel by several users with no collision in transmitting their packets. Plus, all the entire network devices should be known and the number of the devices should be clear because at the initialization of the network TDMA specifies the number of the time slots and the duration of each based on the number of the network devices. A simple example of the TDMA is represented in Figure 5 To illustrate the sequence of the transmission in this protocol[28]. In Figure 5, the Terminal means the connection of the device to the network, as an example, Terminal 1 is the connection of the device 1 and the same for Terminal 2.

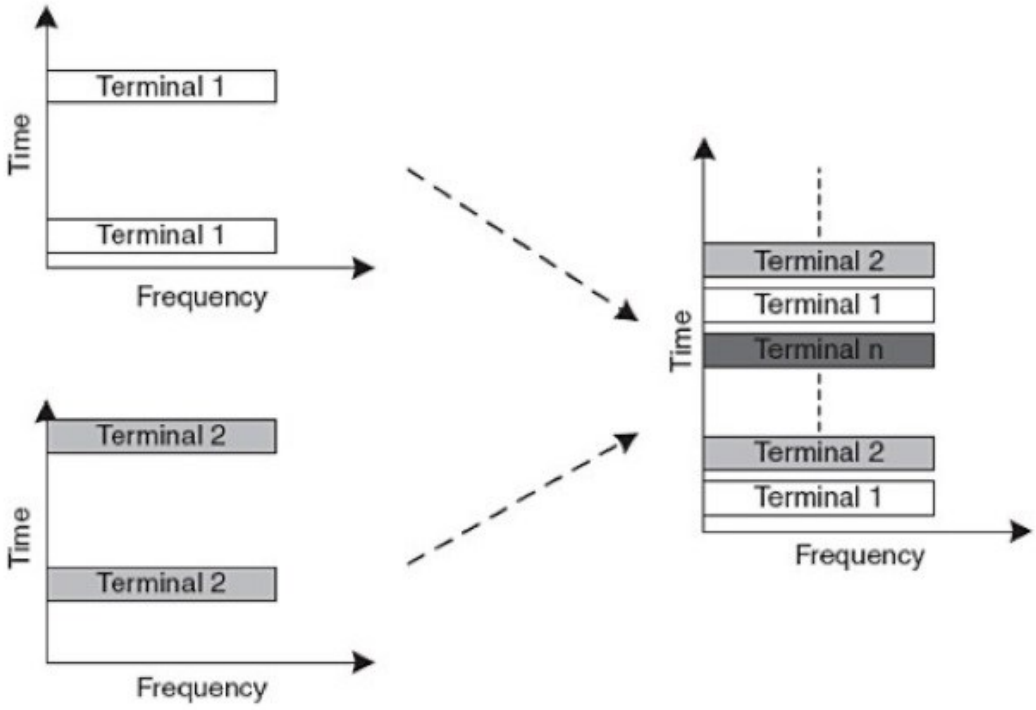

Figure 5. *TDMA packet transmission*[28, Fig. 3.5]

Code Division Multiple Access (CDMA)

This is a channel access method in radio frequency communication technology[28]. In this method, all the entire devices in the network transmit their data packet simultaneously via the same bandwidth.

Spread spectrum systems follow this communication protocol. This technique divides a frequency spectrum of a signal by employing an uncorrelated code with that signal. The division codes have small cross-correlation values and also the code for each user is unique in the network. By considering this feature, the signal is meaningful for the receiver which has the proper code[29],[30].

CDMA has great advantages in growing the efficiency of communication methods. Multi-path effects reduction is one of the pros of applying spread spectrum techniques. Moreover, there is no time limitation for users to start their transmission. The codes are almost random thus the network is more secure. In addition, there is no interference due to the use of the entire frequency spectrum[30].

2.2 UWB Localization Background

This chapter is dedicated to the background of localization techniques which are applied in mobile robots. Localization is an estimation of a robot's location in an external reference frame from sensor data by employing a map of the environment[6, p. 3]. In order to implement the localization, a number of sensors are used which their data are limited to some factors such as noise[6, p. 2]. The noise causes uncertainty in the localization and one of the most important features of a localization algorithm is the robustness against this uncertainty. For localizing a mobile machine a variety of algorithms are applied such as Monte Carlo (Particle Filter), Extended Kalman Filter and Geometric methods[4, p. 2]. In this study, the localization is based on the distance measurement methods and achieved by implementing EKF and Geometric (Trilateration) techniques due to their popularity in industrial subjects, tracking and less mathematical calculation load.

2.2.1 Geometric methods

Geometric is one of the most simplistic methods that is mostly considered due to its simplicity. The geometric method is a process that calculates the location of a target object based on its distance from at least 3 anchor nodes whose locations are determined. All the nodes require an omnidirectional antenna to have good coverage on the test area. Thus the location of the target object is calculated based on the intersection point of at least three spheres that the ranges are the radius and the anchors' positions are the centers of the spheres[31, p. 2]. In the following, the Least Squares Method and a simple Algebraic Solution to the Trilateration will be discussed.

Least Square Estimation (LSE) Method

In this method, the distance between the mobile node and all the anchors are known that is in order to calculate the 3-Dimensional coordinates of the mobile node, at least 4 anchors are required as it is shown in Figure 6. Moreover, there are 5 UWB nodes that one of them is mobile and 4 of them are anchors. Here the N is assumed as the mobile node and its coordinate is (x_N, y_N, z_N) and A1 to A4 as anchor nodes and their coordinates are (x_{P1}, y_{P1}, z_{P1}), (x_{P2}, y_{P2}, z_{P2}), (x_{P3}, y_{P3}, z_{P3}) and (x_{P4}, y_{P4}, z_{P4}). The all measured distances between the mobile

node N and 1st to 4th Anchors are presented with S1 to S4. The mathematical interpretation is such as each anchor is a center of a sphere and the distance to the mobile node is the radius of the sphere. The intersection point of the spheres is the location of the mobile node.

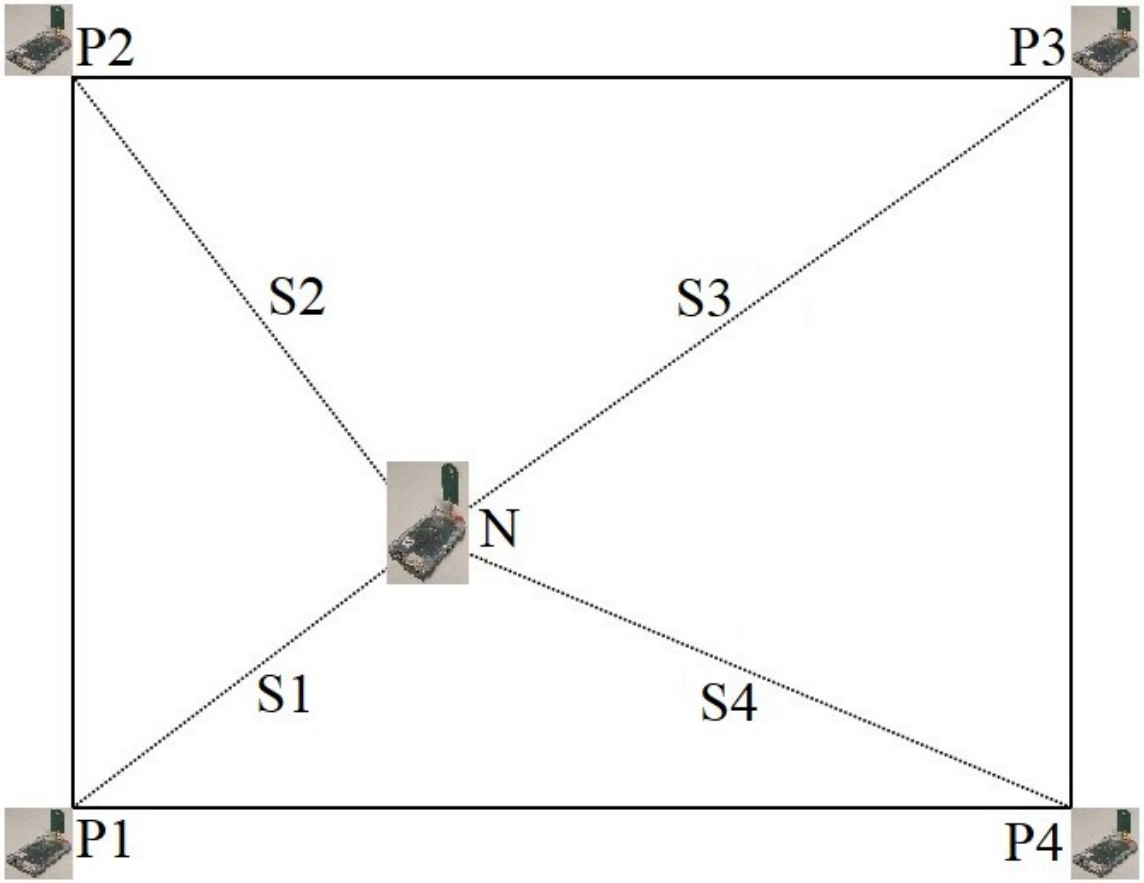

Figure 6. *The Least Square Estimation method with 1 mobile node and 4 anchors*[32, Fig. 28]

Equation (12) is called Observation equations and presents the relationship between the anchors and the mobile node based on their distances and known locations of the anchors.

$$\begin{aligned}
((x_{P1}-x_N)^2+(y_{P1}-y_N)^2+(z_{P1}-z_N)^2)^{\frac{1}{2}} &= S_1 \\
((x_{P2}-x_N)^2+(y_{P2}-y_N)^2+(z_{P2}-z_N)^2)^{\frac{1}{2}} &= S_2 \\
((x_{P3}-x_N)^2+(y_{P3}-y_N)^2+(z_{P3}-z_N)^2)^{\frac{1}{2}} &= S_3 \\
((x_{P4}-x_N)^2+(y_{P4}-y_N)^2+(z_{P4}-z_N)^2)^{\frac{1}{2}} &= S_4
\end{aligned} \tag{12}$$

Siquan et al.[33] mention that when the number of the anchors is 4, it is possible to calculate the exact location while in order to have a more accurate location, the number of anchors should be more than 4. In this condition, we have a non-linear group of the equations which will be solved by applying simple LSE method.

A simple LSE algorithm can be influenced easily by ranging error. In addition, this method finds the solutions by subtracting the n^{th} equation from the 1st equation, plus the accuracy of the solution is influenced by the precision of the n^{th} equation. LSE first uses the Taylor series expansion in order to linearize the non-linear observation equations. One of the detriments of this method is providing its requirement to the coordinate estimation of the initial location[33]. The equations of the algorithm are illustrated in the (13) and (15)[33]:

$$f_{Pi}(x_N, y_N, z_N) = ((x_{Pi+1} - x_N)^2 + (y_{Pi+1} - y_N)^2 + (z_{Pi+1} - z_N)^2)^{\frac{1}{2}} - ((x_{P1} - x_N)^2 + (y_{P1} - y_N)^2 + (z_{P1} - z_N)^2)^{\frac{1}{2}} \quad (13)$$

$$f_{Pi}(x_N, y_N, z_N) = d_{Pi} + \varepsilon_i \quad (14)$$

n denotes the number of the anchor nodes.

i is a variable between 1 to $n - 1^{th}$ anchor nodes.

$f_{Pi}(x_N, y_N, z_N)$ denotes subtraction function of the range measurement between the 1st, the $i + 1^{th}$ anchor nodes and the mobile node.

d_{Pi} denotes the estimated distance difference between the 1st, the $i + 1^{th}$ anchor node and the mobile node.

ε_i means the covariance matrix of the calculated distance difference error.

$\Delta = \begin{bmatrix} \Delta x \\ \Delta y \\ \Delta z \end{bmatrix}$ denotes the estimation of changes in the position.

By assuming $(x_{init}, y_{init}, z_{init})$ as the initial position estimation then the position coordinate could be as equation (15)[33]:

$$\begin{aligned} x_N &= x_{init} + \Delta x \\ y_N &= y_{init} + \Delta y \\ z_N &= z_{init} + \Delta z \end{aligned} \quad (15)$$

By expanding the function $f_{Pi}(x_N, y_N, z_N)$ via the Taylor series, and retaining the first two terms as it is presented in the equation (16)[33]:

$$f_{Pi,init} + \alpha_{Pi,1}\Delta x + \alpha_{Pi,2}\Delta y + \alpha_{Pi,3}\Delta z \approx d_{Pi} + \varepsilon_i \quad (16)$$

Then we have,

$$f_{Pi,N} = f_{Pi}(x_N, y_N, z_N) \tag{17}$$

$$\begin{cases} \alpha_{Pi,1} = \dfrac{\partial f_{Pi,N}}{\partial x_N} | x_{init}, y_{init}, z_{init} = \dfrac{x_{P1} - x_{init}}{d_{P1}} - \dfrac{x_{Pi+1} - x_{init}}{d_{Pi+1}} \\ \alpha_{Pi,2} = \dfrac{\partial f_{Pi,N}}{\partial y_N} | x_{init}, y_{init}, z_{init} = \dfrac{y_{P1} - y_{init}}{d_{P1}} - \dfrac{y_{Pi+1} - y_{init}}{d_{Pi+1}} \\ \alpha_{Pi,3} = \dfrac{\partial f_{Pi,N}}{\partial z_N} | x_{init}, y_{init}, z_{init} = \dfrac{z_{P1} - z_{init}}{d_{P1}} - \dfrac{z_{Pi+1} - z_{init}}{d_{Pi+1}} \end{cases} \tag{18}$$

$$\begin{aligned} d_{Pi} = ((x_N - x_{Pi})^2 + (y_N - y_{Pi})^2 + (z_N - z_{Pi})^2)^{1/2} \\ - ((x_N - x_{P1})^2 + (y_N - y_{P1})^2 + (z_N - z_{P1})^2) \end{aligned} \tag{19}$$

The weighted least squares estimate of equations (16), (17), (18) and (19) is expressed as equation (20)[33]:

$$A\Delta = D + e \tag{20}$$

$$A = \begin{bmatrix} \alpha_{P1,1} & \alpha_{P1,2} & \alpha_{P1,3} \\ \vdots & \vdots & \vdots \\ \alpha_{Pn-1,1} & \alpha_{Pn-1,2} & \alpha_{Pn-1,3} \end{bmatrix}, \Delta = \begin{bmatrix} \Delta x \\ \Delta y \\ \Delta z \end{bmatrix}, D = \begin{bmatrix} d_{P1} - f_{P1,init} \\ \vdots \\ d_{Pn} - f_{Pn,init} \end{bmatrix}, e = \begin{pmatrix} \varepsilon_{2,1} \\ \vdots \\ \varepsilon_{n,1} \end{pmatrix}, i = 1,2, \dots n-1 \tag{21}$$

And finally rewriting equation (20) such as equation (22)[33]:

$$\Delta = \left[A^T A\right]^{-1} A^T D \tag{22}$$

$$x_{init} + \Delta x \to x_{init} \quad , \quad y_{init} + \Delta y \to y_{init} \quad , \quad z_{init} + \Delta z \to z_{init} \tag{23}$$

Based on the equation (22), Δ is computed according to the initial position $(x_{init}, y_{init}, z_{init})$ and the position of the anchors. Then, it will be added to the initial position and updates it iteratively according to the equation (23) till achieving the intended accuracy or the maximum times of the permitted iteration. The last value of $(x_{init}, y_{init}, z_{init})$ in the last iteration is the position coordinate of the mobile node (x_N, y_N, z_N)[33].

The algorithm of this method, in brief, is as follows:

1: The initial position coordinate is calculated by Observation equations
2: **while** mean(e) > desired accuracy or maximum number of iteration
3: **for** i = number of the Anchor nodes
4: (18),(19),(21),(22),(23)
5: **end for**
6: **end while**

Trilateration

Most of the position estimation algorithms are complicated and need extensive computation capabilities while in real-time cases or some devices with restricted hardware capability such as sensor nodes a fast and accurate algorithm is required. Norrdine et al.[34] offers a simple algebraic solution for the trilateration problem. This method is a solution to find the unknown position of a target object (Mobile node) in a 3D environment based on its distances from the 3 reference nodes (anchors) with known positions as it is illustrated in Figure 7. This algorithm does not follow iteration or approximation methods. It treats the nonlinear elements of the equations system as extra unknown elements that they illustrate a constraint simultaneously. Therefore, it builds a new equations system based on the old one and the aforementioned solution is based on the mean of linear algebra methods with light computational load[34].

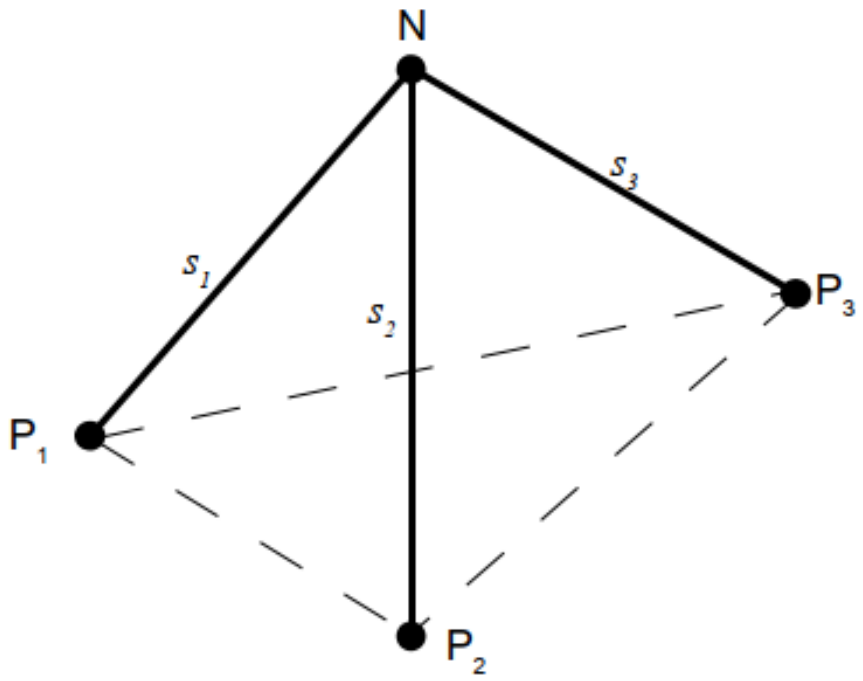

Figure 7. *3 anchors (P1, P2, P3) and one mobile node (N) in Trilateration problem*[34]

The notation used in trilateration:

$\{P_1(x_{p1}, y_{p1}, z_{p1}), P_2(x_{p2}, y_{p2}, z_{p2}), P_3(x_{p3}, y_{p3}, z_{p3})\}$ – Denote coordinate of the 3 anchors at $\{I\}$

$\{s_1, s_2, s_3\}$ – Mean range measurements between the mobile node and each of the three anchors at $\{I\}$

$\{N(x_N, y_N, z_N)\}$ – Denotes coordinate of the mobile node at $\{I\}$

The coordinate of the Mobile node $N(x_N, y_N, z_N)$ will be calculated by solving the quadratic equation system in equations (24).

$$\begin{cases} (x_{p1} - x_N)^2 + (y_{p1} - y_N)^2 + (z_{p1} - z_N)^2 = s_1^2 \\ (x_{p2} - x_N)^2 + (y_{p2} - y_N)^2 + (z_{p2} - z_N)^2 = s_2^2 \\ (x_{p3} - x_N)^2 + (y_{p3} - y_N)^2 + (z_{p3} - z_N)^2 = s_3^2 \end{cases} \tag{24}$$

Equation (24) can be rearranged as equation (25):

$$\begin{cases} (x_N^2 + y_N^2 + z_N^2) - 2x_{p1}x - 2y_{p1}y - 2z_{p1}z = s_1^2 - x_{p1}^2 - y_{p1}^2 - z_{p1}^2 \\ (x_N^2 + y_N^2 + z_N^2) - 2x_{p2}x - 2y_{p2}y - 2z_{p2}z = s_2^2 - x_{p2}^2 - y_{p2}^2 - z_{p2}^2 \\ (x_N^2 + y_N^2 + z_N^2) - 2x_{p3}x - 2y_{p3}y - 2z_{p3}z = s_3^2 - x_{p3}^2 - y_{p3}^2 - z_{p3}^2 \end{cases} \tag{25}$$

Or it can be shown in matrix form as equation (26):

$$\begin{bmatrix} 1 & -2x_{p1} & -2y_{p1} & -2z_{p1} \\ 1 & -2x_{p2} & -2y_{p2} & -2z_{p2} \\ 1 & -2x_{p3} & -2y_{p3} & -2z_{p3} \end{bmatrix} \begin{bmatrix} x_N^2 + y_N^2 + z_N^2 \\ x \\ y \\ z \end{bmatrix} = \begin{bmatrix} s_1^2 - x_{p1}^2 - y_{p1}^2 - z_{p1}^2 \\ s_2^2 - x_{p2}^2 - y_{p2}^2 - z_{p2}^2 \\ s_3^2 - x_{p3}^2 - y_{p3}^2 - z_{p3}^2 \end{bmatrix} \tag{26}$$

Therefore, (26) is shown in the following form (27):

$$A_0 \cdot X = b_0 \tag{27}$$

Where $X \in E$ and $E = \{(x_0, x_1, x_2, x_3)^T \in \mathbb{R}^4 / \, x_0 = x_1^2 + x_2^2 + x_3^2\}$

Thus the general solution of equation (27) stands as (28):

$$X = X_p + t \cdot X_h \tag{28}$$

With the real parameter t where X_p is a specific solution of the equation (28) and X_h is a solution to the homogeneous system $A_0 \cdot X = 0$ [34].

In order to calculate the X_p and X_h, Gaussian Elimination method can be applied. The specific value of the X_p is possible to be calculated by the minimum norm of the pseudo-inverse of the matrix A_0 [34].

Computation of the parameter t stands according to the X_p, X_h and X via the values are shown in (29).

By inserting (29) into (28) it becomes (30):

$$\begin{aligned} X_p &= \left(X_{p0}, X_{p1}, X_{p2}, X_{p3}\right)^T \\ X_h &= (X_{h0}, X_{h1}, X_{h2}, X_{h3})^T \\ X &= (x_0, x_1, x_2, x_3)^T \end{aligned} \tag{29}$$

$$\begin{cases} x_0 = X_{p0} + t \cdot X_{h0} \\ x_1 = X_{p1} + t \cdot X_{h1} \\ x_2 = X_{p2} + t \cdot X_{h2} \\ x_3 = X_{p3} + t \cdot X_{h3} \end{cases} \tag{30}$$

By employing the constraint $X \in E$ it converts to the (31).

$$X_{p0} + t\,.X_{h0} = \left(X_{p1} + t \cdot X_{h1}\right)^2 + \left(X_{p2} + t \cdot X_{h2}\right)^2 + \left(X_{p3} + t \cdot X_{h3}\right)^2 \tag{31}$$

By simplification, it turns to (32):

$$\begin{aligned} t^2(X_{h1}^2 + X_{h2}^2 + X_{h3}^2) + t\left(2 \cdot X_{p1}X_{h1} + 2 \cdot X_{p2}X_{h2} + 2 \cdot X_{p3}X_{h3} - X_{h0}\right) + X_{p1}^2 + X_{p2}^2 \\ + X_{p3}^2 - X_{p0}^2 = 0 \end{aligned} \tag{32}$$

Thus now it is a simple quadratic equation such as $at^2 + bt + c = 0$ and the solution is in (33):

$$t_{1,2} = \frac{-b \pm \sqrt{b^2 - 4ac}}{2a} \tag{33}$$

Therefore, the solutions of the equation (27) are (34):

$$\begin{aligned} X_1 &= X_p + t_1 \cdot X_h \\ X_2 &= X_p + t_2 \cdot X_h \end{aligned} \tag{34}$$

In short distances, the Trilateration problem might face some problems and also no real solutions could be found. In such cases, the real part could be considered as an approximation to the solution and the constraint $X_{1,2} \in E$ is not satisfied. Consequently, the difference between x_0 and $(x_1^2 + x_2^2 + x_3^2)$ is called Solvability factor in this study and it indicates whether the calculation is valid or not(35)[34]:

$$Solvability = x_0 - (x_1^2 + x_2^2 + x_3^2) \tag{35}$$

When the value of the Solvability is zero the constraint condition is met and the solution is valid. The N_1 and N_2 are the Trilateration problem solutions (36):

$$I = \begin{bmatrix} 0 & 0 & 0 & 0 \\ 0 & 1 & 0 & 0 \\ 0 & 0 & 1 & 0 \\ 0 & 0 & 0 & 1 \end{bmatrix}, N_1 = X_1 \cdot I, N_2 = X_2 \cdot I \tag{36}$$

The aforementioned method does not propose a method to calculate the variance of the N_1 and N_2. In the geometric method, the mobile node is assumed as stationary in the moment of the location computation. Thus the variance of the N_1 and N_2 could be computed by the following method.

$$R = \begin{bmatrix} \sigma_x^2 & 0 & 0 \\ 0 & \sigma_y^2 & 0 \\ 0 & 0 & \sigma_z^2 \end{bmatrix} \tag{37}$$

$$r_1 = \begin{bmatrix} x_N - x_{p1} \\ y_N - y_{p1} \\ z_N - z_{p1} \end{bmatrix}, r_2 = \begin{bmatrix} x_N - x_{p2} \\ y_N - y_{p2} \\ z_N - z_{p2} \end{bmatrix}, r_3 = \begin{bmatrix} x_N - x_{p3} \\ y_N - y_{p3} \\ z_N - z_{p3} \end{bmatrix} \tag{38}$$

The measurement equation is $h(x, y, z)$ which describes the measured range based on the position of the mobile node and a specific anchor as shown in equation (39), i is the number of the anchor P:

$$h(x_N, y_N, z_N) = \left(\left(x_N - x_{pi}\right)^2 + \left(y_N - y_{pi}\right)^2 + \left(z_N - z_{pi}\right)^2 \right)^{\frac{1}{2}} \tag{39}$$

Thus the distances between the mobile node and the anchors are such as equation (40):

$$S_1 = \sqrt{r_1^T * r_1}, \qquad S_2 = \sqrt{r_2^T * r_2}, \qquad S_3 = \sqrt{r_3^T * r_3} \tag{40}$$

Then, the Jacobian of the $h(x_N, y_N, z_N)$ with respect to the (x_{Pi}, y_{Pi}, z_{Pi}) for each reference point (anchors) in equation (41):

$$H = \frac{\partial h(x_N, y_N, z_N)}{\partial x}\Big|_{x=(x_N, y_N, z_N)} = \begin{bmatrix} \frac{x_N - x_{p1}}{S_1} & \frac{y_N - y_{p1}}{S_1} & \frac{z_N - z_{p1}}{S_1} \\ \frac{x_N - x_{p2}}{S_2} & \frac{y_N - y_{p2}}{S_2} & \frac{z_N - z_{p2}}{S_2} \\ \frac{x_N - x_{p3}}{S_3} & \frac{y_N - y_{p3}}{S_3} & \frac{z_N - z_{p3}}{S_3} \end{bmatrix} \tag{41}$$

And the values of the main diagonal of the var_{uwb} in the equation (42) are the variance values of (x_N, y_N, z_N):

$$var_{uwb} = H * R * H^T \tag{42}$$

2.2.2 Extended Kalman Filter (EKF)

Extended Kalman Filter predicts the posterior state of a nonlinear dynamic system based on the prior state and then updates the posterior states by receiving true data from external resources[35].

At the beginning of this chapter, a short description regarding an important feature of a localization algorithm in the way it deals with sensor noise is mentioned. Extended Kalman Filter is a probabilistic localization method which considers uncertainty in its algorithm. EKF notices uncertainty in its measurement model by using probability distribution[6, p. 3]. Probability distribution (Gaussian Function) illustrates the uncertainty as vectorized Normal distribution which is called multivariate normal distribution with μ as mean vector and ∑ which is a symmetric matrix as covariance matrix[6, p. 10,11]. Figure 8 graphically illustrates a normal distribution with scalar values for mean $\mu = 0$ and variance $\sigma^2 = 1$.

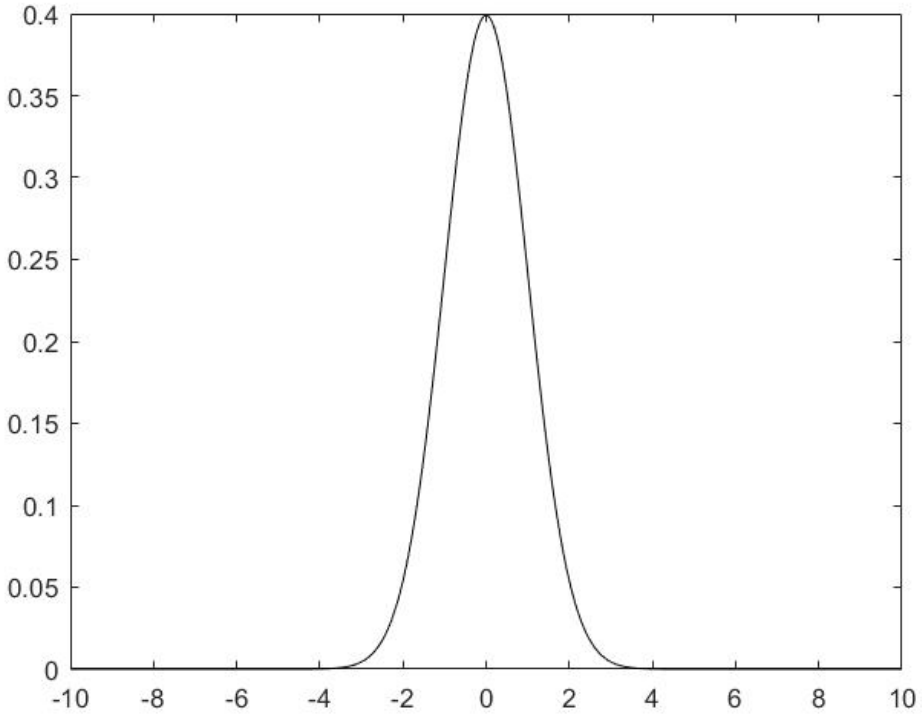

Figure 8. *Normal Distribution with mean $\mu = 0$ and variance $\sigma^2 = 1$*

Complementary information regarding probabilistic theories and Gaussian Filters can be found in[6, Ch. 2,3]. In this thesis, 2 EKF algorithms are implemented which will be described in the next chapter in details. However, a general explanation of the EKF is presented in the following.

The pose is referred to the position and orientation of a rigid body. Pose in a 3D space consists of 6 variables (3 cartesian coordinates which are x, y, z or North, East and Down and 3 angular orientation which are roll, pitch, and yaw). The pose is required in order to specify the exact location of a target object in a 3D space.

EKF consists of 2 steps which are prediction step and update step. The prediction step predicts the posterior states and the relative covariance. It contains a motion model and a measurement model. The motion model is an equation system which is applied in state transition[6, p. 93]. Motion model is categorized to 2 types which are velocity motion model and odometry motion model. The velocity motion model employs the rotational and translational velocity to calculate posterior state over the pose while the odometry motion model calculates the posterior based on the odometry measurements. It calculates the traveled distance by integrating wheel encoders information[6, p. 107]. The measurement model contains an equation system which is used to predict the posterior measurement. In the prediction step, the uncertainty will increase [6, p. 39].

The update step integrates the measurement data into the predicted values of the state and covariance; in addition, it decreases the uncertainty[6, p. 39]. In the following, equations (43) to (53) present the EKF[36, p. 310]:

Nonlinear Dynamic (Motion) Model in equation (43):

$$x_k = \phi_{k-1}(x_{k-1}, u_k) + \epsilon_{k-1}, \quad \epsilon_K \sim \mathcal{N}(0, Q_k) \tag{43}$$

Nonlinear Measurement Model in equation (44):

$$z_k = h_k(x_k) + \theta_k, \quad \theta_k \sim \mathcal{N}(0, R_k) \tag{44}$$

Prediction step of motion model and measurement model are depicted in equations (45) and (46):

$$\hat{x}_k(-) = \phi_{k-1}(x_{k-1}(+), u_k) \tag{45}$$

$$\hat{z}_k = h_k(\hat{x}_k(-)) \tag{46}$$

In order to predict the state covariance, the motion model is linearized by the first Taylor series expansion in equation (47):

$$\Phi_{k-1} = \frac{\partial \phi_k}{\partial x}|_{x=x_{k-1}(+)} \tag{47}$$

Q_k and L_c will be calculated by (48):

$$Q_k = ts * L_c Q_c L_c^T, \quad L_c = \frac{\partial \phi_k}{\partial \epsilon}|_{\epsilon=0} \tag{48}$$

L_c denotes the Jacobian of the motion model with respect to the control noise vector in order to linearize the control noise. $\{\epsilon\}$ is hidden within the $\{u_k\}$ [37].

Prediction of the covariance matrix is shown in equation (49):

$$P_k(-) = \Phi_{k-1} P_{k-1}(+) \Phi_{k-1}^{\mathrm{T}} + Q_{k-1} \tag{49}$$

Linearization of the measurement model by first Taylor series expansion is done in equation (50) and computation of the Kalman Gain in equation (51):

$$H_{k-1} = \frac{\partial h_k}{\partial x}|_{x=\hat{x}_k(-)} \tag{50}$$

$$K_k = P_k(-) H_k^T (H_k P_k(-) H_k^T + R_k)^{-1} \tag{51}$$

Update step updates the state and covariance matrix which are shown in the equations (52) and (53) when a new measurement data is received:

$$\hat{x}_k(+) = \hat{x}_k(-) + K_k(z_k - \hat{z}_k) \tag{52}$$

$$P_k(+) = (I - K_k H_k) P_k(-) \tag{53}$$

Notations used in EKF equations:

$\{x_k\}$ – State of the system

$\{\hat{x}_k\}$ – Predicted state of the system

$\{z_k\}$ – Measurement

$\{\hat{z}_k\}$ – Predicted measurement

$\{\phi_k\}$ – Motion model

$\{u_k\}$ – Control vector

$\{\Phi_k\}$ – Jacobian of motion model with respect to the state vector

$\{\epsilon_K\}$ – Process noise

$\{h_k\}$ – Measurement Model

$\{H_k\}$ – Jacobian of the measurement model with respect to the state vector

$\{\theta_k\}$ – Measurement noise

$\{P_k\}$ – Covariance of the state

$\{K_k\}$ – Kalman Gain

$\{Q_k\}$ – Process noise covariance

$\{\epsilon\}$ – Control noise vector, it is hidden in the control vector

$\{L_c\}$ – Jacobian of Motion model with respect to the control noise vector

$\{Q_c\}$ – Control noise covariance

$\{R_k\}$ – Measurement noise covariance matrix

$\{ts\}$ – Time stamp

2.3 DEVICE CHARACTERISTICS

The employed UWB device in this thesis is a PulsON 440 (P440) module which is an Ultra-Wideband radio transceiver with an operational frequency range between 3.1 and 4.8 GHz. It is a member of the P400 series of TimeDomain UWB platform and supports the three mentioned applications of the UWB in the previous chapter which are Positioning, radar and communications[38, p. 5].

P440 has the capability of setting up a network in aforementioned applications via at least between 2 and maximum among 10 devices due to the software restriction by the company while the commercial version of the P440 does not suffer from this restriction. Not only does this device support the ALOHA and TDMA protocols, but also it is capable of communicating via a maximum of 11 different channels because of a CDMA-based network. A location engine specifies a 2D(X, Y) or 3D(X, Y, Z) position based on Kalman Filter or Geometric (Nonlinear Least Squares) method via employing ranging measurement. The design of the hardware is compatible with the industrial environment and can operate in noisy, high shock and vibration environment with $-40℃$ to$+85℃$. In order to range measurement, it employs the TWR or TW-TOF. The power consumption per transmission is $50\mu W$[39].

The P440 is a coherent radio transceiver which means for increasing the Signal to Noise Ratio (SNR) of the captured signals, it sums up the energy in each transmitted pulse. By raising the number of sent pulses to twice, the SNR will increase by $3\ dB$ while it also grows the time of transmission[39].

P440 could be used in three different applications:

1. Ranging and Network (RangeNet)
2. Monostatic Radar
3. Bistatic/Multistatic Radar and Channel Analysis

The manufacturer company presents a Graphical User Interface as a tool for each application separately which not only makes the end-user able to configure the device simply but also illustrates the way each application works.

In this thesis, the Ranging and Network application is applied. Figure 9 presents The P440 module. This device supports two antennas yet it working normally by one antenna and can operate all of the applications[39].

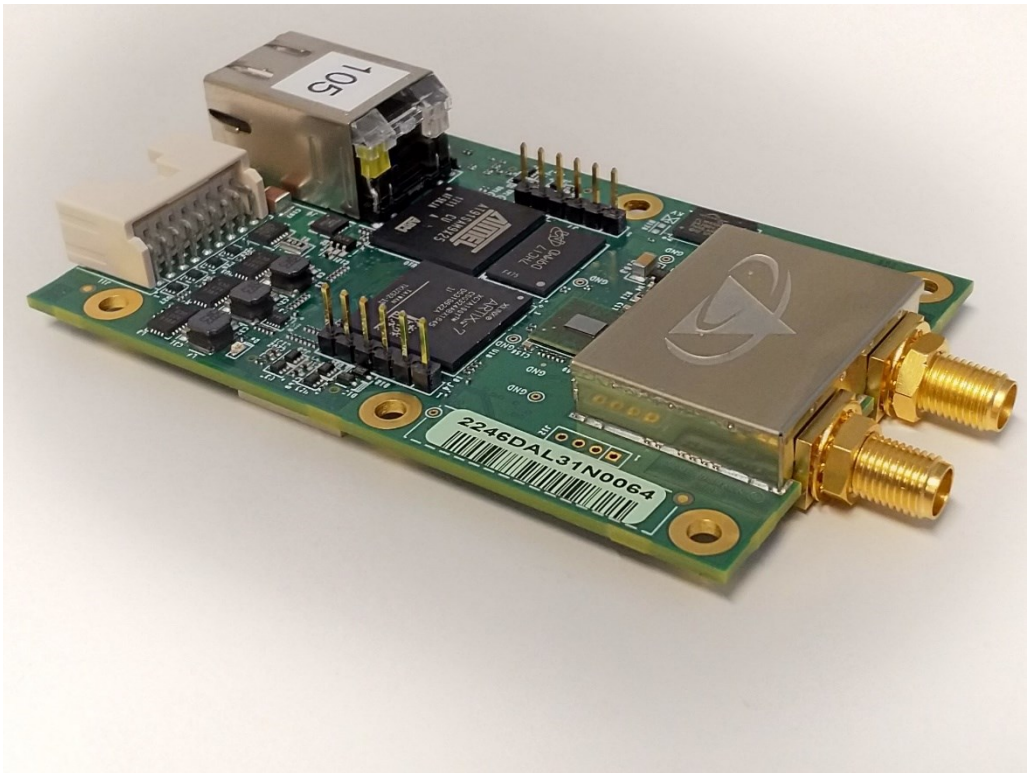

Figure 9. *The P440 UWB device*

2.3.1 Connecting to P440

There are various ways to connect to the P440. A view of the connectors is illustrated in Figure 10.

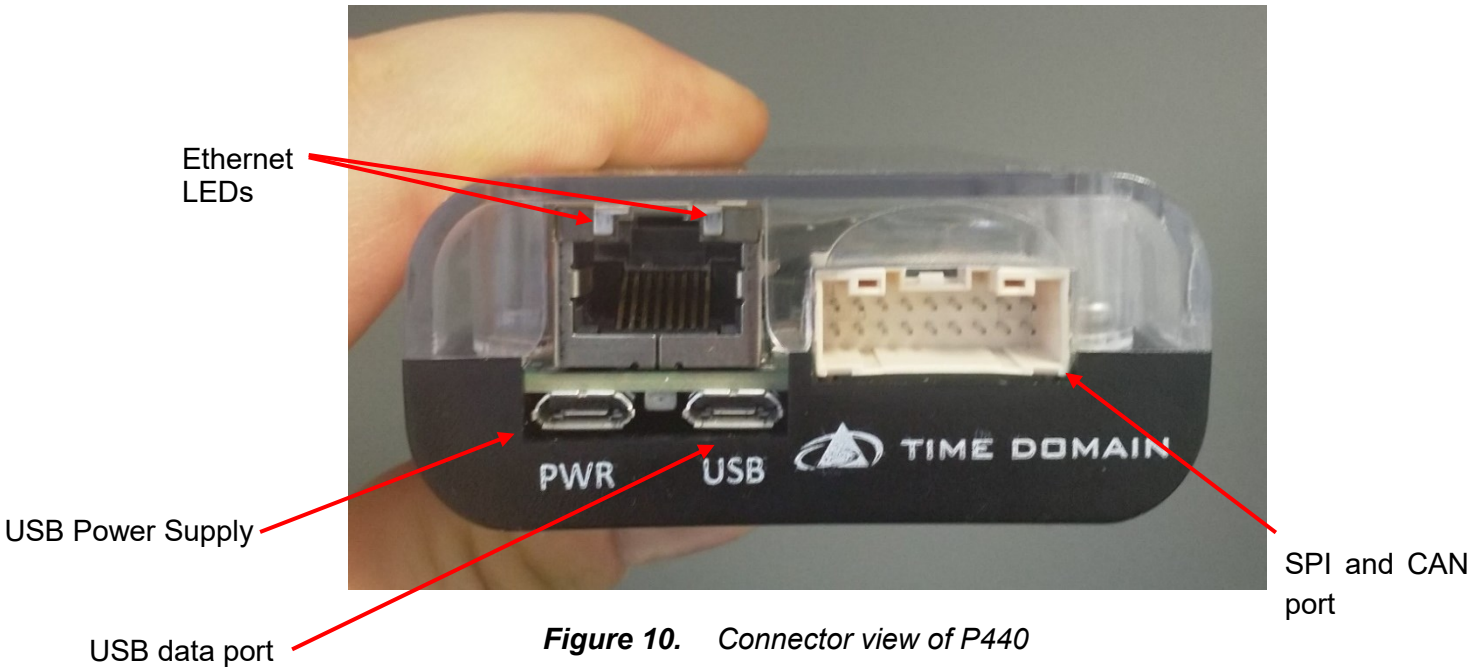

Figure 10. *Connector view of P440*

As it can be seen in Figure 10, P440 equipped by 2 USB ports, one Ethernet and a pin port with 18 pins which are employed to communicate via SPI or CAN protocols. They are described in the following[39].

USB Port

As it is illustrated in Figure 10, the PWR USB port is the USB power supply jack and should be connected to the USB power supply or the USB battery. The power supply could be varied between 5 and 48 DC Volts[39, p. 35]. The USB data port is another connection type of P440. The USB port connects via a USB data jack. The highest data rate for this port is 480 Mbps.

Each device owns a node ID which starts from 100 and ends the last one such as 109 when there are 10 modules. The node ID should be unique for each device and if there are two devices with the same node ID collision will happen in their data frames. The node ID could also be modified via the proper GUI[39].

The Ethernet port

An Ethernet 10/100 port supports 10 to 100 Mbps which let the P440 connect to a host computer via an RJ45 jack. The communication speed of the device is

restricted by several factors such as the Ethernet protocol and the processing capability of the host computer.

In order to communicate with the device via Ethernet, an IP address in a local network should be allocated to each device. For instance, 192.168.1.100 is the IP address for the device with node ID 100 and 192.168.1.109 is the IP address for the device with node ID 109. The provided GUI by the manufacturer gives the end-user capability of configuring the IP address. However, in order to prevent data frames collision, the IP addresses must be unique.[39].

Serial Peripheral Interface (SPI)

One of the methods of communication with this device is SPI and the highest clock rate for this communication port is 16 MHz, however, its actual data rate is 6 to 7 Mbps. The higher performance of this type of communication could be achieved by shortening the length of the communication link as less as possible. The maximum length of the cable when the device operates at 16 MHz is no longer than 15 cm, plus, the provided GUI by the manufacturer makes the end-user capable of configuring the communication[39]. There is more information about this method of communication in the datasheet of the device.

Controller Area Network (CAN)

Controller Area Network is a serial communication protocol. The CAN interface of P440 follows the J1939 protocol. This protocol is based on CAN 2.0B and provides a high speed and reliable communication system. More information regarding the J1939 protocol can be found [40], [41]. This device is capable of communicating via various baud-rate from 1 Kbps to 1 Mbps. Moreover, each node must have an address to be recognizable. The end-user can configure the CAN communication method via the provided GUI[39].

The regular way of communication with this device is via the Ethernet port. In order to have more information about CAN or SPI network protocols, the Data Sheet PDF file of the device has a complete description[38, p. 27,37].

2.3.2 Indicator Lights

As can be observed in Figure 10 and Figure 11, the device is equipped with 5 LEDs to indicate the situation of the network, transmission of the data and main processing unit.

Ethernet LEDs

Ethernet port is equipped with 2 different LEDs that are shown in Figure 10 and they are used to illustrate the situation of the port.

1. Green: In Off mode means the network is 10 Mbps and in another situation means the network is 100 Mbps.
2. Yellow: This LED could be On, Off and blink which respectively means the network is available, no network and regular data transmission.

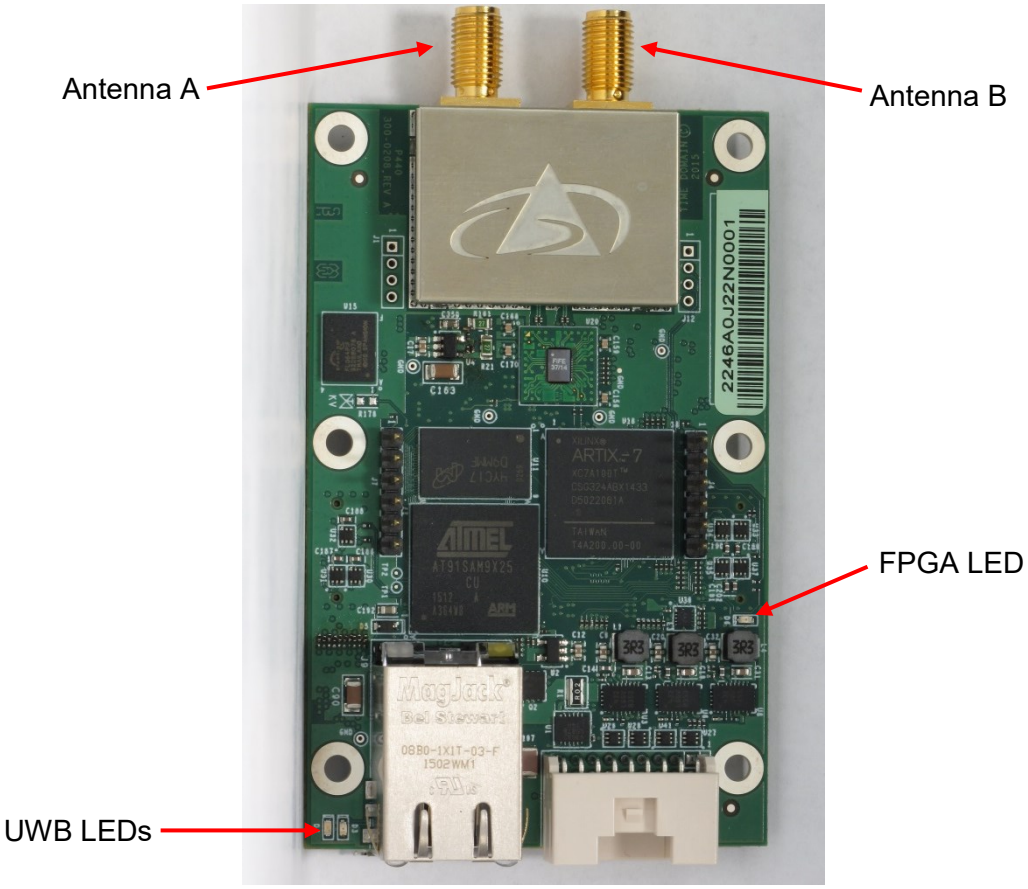

Figure 11. *Antennas and Indicator lights of P440*

UWB LEDs

Two LEDs are provided to illustrate the operating condition of the device and the transmission of data among devices of the networks. These LEDs have two situations, On and Off.

1. Blue: When the unit is in the boot condition this LED is on and solid. In a normal situation, it blinks by 0.5 Hz. If after booting it turns off or remains lit solid, the unit is faulty.
2. Green (UWB activity): This LED after boot of the device should be lit. If the unit has data transmission with other units in any application this LED should blinking and the rate of the blinking depends on the data transmission rate. For instance, if the unit receives the range data of the 9 other devices in a network the frequency of each cycle will be 4.60 Hz and the LED blinks by 41.4 Hz. In case, the device is on and there is no device in the device network, the LED should be lit solid, otherwise, it is faulty.

FPGA LED

FPGA is the microcontroller of the device. Since the power supply is connected to the unit it should blink and it means the device is prepared to operate in the configured mode and start the data transmission. If the LED lit or off solid, it means a faulty FPGA.

In the following, the operations of the UWB and FPGA LEDs are described In brief. When the power supply is provided to the unit, the FPGA LED starts to blink by 2 Hz rate. Meanwhile, the blue LED of the UWB also is on solid for 8 seconds during the boot process of the device and if the device boots normally, the blue LED will blink by 0.5 Hz.

If one of the bellow conditions occurred the device is faulty[38, p. 45]:

- The UWB turned on solid blue LED does not start to blink by 0.5 Hz after boot.
- After boot, the UWB blue LED starts to blink by 2 Hz.
- The FPGA green LED does not blink by 2 Hz rate.

- Generally, if any situation except the normal boot process happens, it means that the device is faulty.

2.3.3 Broadspec Antenna

The P440 communication tool in the entire applications is the Broadspec antenna. As it is illustrated in Figure 11, P440 has 2 Antenna connection ports. Configuration of the antenna in Ranging and Networking application has no effect on the performance of the UWB device while the objects and environment characteristics can vary the efficiency of the device in Radar application, thus the antenna requires to be configured based on the aforementioned factors. However, in the setting, the antenna type should be configured (to apply Antenna A, B or both) and it should be connected to the device based on the configuration. The P440 Broadspec Antenna is shown in Figure 11. As the figure represents, the range measurements between the units are exactly the distance between the phase centers of the Broadspec Antenna of the relative units. The original antenna is replaceable with a custom one with consideration to the resistance of the SubMiniature version A (SMA) connection of the antenna, which is 50 ohms and the EU standards because by applying new antenna the beam pattern and the gain will be changed.

Figure 12. *Broadspec antenna with the Phase Center indication*

2.3.4 Range measurement

P440 provides 1 range measurement and 2 range estimation values. Precision Range Measurement (PRM) is the main range measurement which measures the

distance between 2 units of P440 by TW-TOF method. The range estimations are Coarse Range Estimate (CRE) and the Filtered Range Estimate (FRE). CRE is a raw coarse distance substantiated on a direct path of the signal strength and its value changes based on the PRM value. FRE is the result of an optimal estimator such as Kalman filter in the device firmware. These 2 estimators are not described more since they are not related to this study, but more information regarding them could be found in[42, p. 149,150].

2.3.5 Maximum operating range

The maximum range of the P440 could be extremely affected by the environment features, the height of the reference units' antenna from the ground and the soil condition (wet or dry).

The maximum range of the device is possible to be tuned by configuring a parameter in the device which is called Pulse Integration Index (PII). Pulse Integration is a method to enhance the accuracy of the measurement via multiplication of a number of received signals from each reference to almost neutralize the effects of the impulsive interferences[43]. The PII in P440 device could be varied between 4 and 9. In Table 1, the numbers of multiplied signals and the maximum range in the open field and free space are illustrated. The larger PII values mean a higher SNR, a longer-range operation with a slower rate in ranging and data communication.

PII	Number of integrated pulses per measurement	Max Range (m) (Free Space)	Max Range (m) (Open Field)
4	16:1	66	-
5	32:1	101	-
6	64:1	145	-
7	128:1	207	500
8	256:1	260	600
9	512:1	410	800

Table 1. *The maximum range of P440 in Open Field and Free Space by various values of PII and the number of pulses per measurement*[38, p. 60]

2.3.6 Range measurement rate

The range measurement rate is configured based on the PII. By increasing PII, the rate will decline and vice versa as it is shown in Table 2. For instance, if the

PII = 7, each P440 unit in the network has 21.2 millisecond time to transmit the data frame.

PII	Range Conversation Time (ms)	Maximum Range Measurement Rate (Hz)
4	8.1	123.5
5	9.8	102.0
6	13.8	72.5
7	21.2	47.2
8	36.4	27.5
9	67.3	14.9

Table 2. *The data rate of P440*[38, p. 61]

2.3.7 Data communication rate

The data communication via P440 is provided only in ranging application. The maximum number of bytes per packet is restricted to 1000 by the manufacturer. Table 3 presents the relation between PII and packet sizes in 100 and 1000 bytes. It should be mentioned that the bit-rate will vary via applying various channels in a few percents [38, p. 67].

	Bytes sent using Code Channel 2	
	100	1000
PII	Bit-rate (kbps)	Bit-rate (kbps)
4	270.46	612.48
5	192.77	308.48
6	138.56	144.64
7	62.14	76.80
8	34.88	39.04
9	17.41	19.20

Table 3. *The data transmission rate for different PII and packet sizes*[38, p. 66]

2.3.8 Ranging, Networking, and Positioning

One of the applications of the P440 is localization which contains measurement of the distance between 2 devices (Ranging) or among several devices (Networking) or finding the location of a P440 mobile device based on the location

of some P440 reference devices (anchors) with specific locations (Positioning). In the following, the entire applications will be described.

Ranging

Ranging function is the simplest application of the P440 and it could be applied just between two devices. In order to implement the range measurement application, both devices should be configured by the same Pulse Integration Index and operate in the identical Code Channel.

The ranging message contains below information:

1. Message-ID: requester assigns it to the request message and the responder returns it in the response message.
2. Source Node ID or Responder ID: is the Node ID of the UWB module which sent the range response.
3. Noise: shows the noise value which is generated in the receiver from the received signal.
4. Vpeak: is the scaled estimate of the maximum received signal in the leading edge as measured by the device. PRMs and CREs update it.
5. Requester and Responder Antenna: reveal the number and mode of antennas in the requester and responder node.
6. Stopwatch Time: is the length of the conversation.
7. Range Status: illustrates the status of the message. 0 means a healthy message; otherwise, the message is corrupted.
8. Leading-Edge Detection Flags: is one of the most important parameters which indicates the situation of the measurement whether it is normal, saturated, LOS or NLOS measurement or any problem in phase or any other problem in characteristics of the received measurement.
9. PRM
10. CRE
11. FRE
12. PRM Error: Error value of the PRM
13. CRE Error: Error value of the CRE
14. FRE Error: Error value of the FRE

15. FRV: is the velocity that illustrates the 2 devices are getting closer or farther to each other. The positive velocity means receding and the negative one means approaching. Its measurement unit is millimeter per second.
16. FRV Error: Error value of the FRV

Additionally, by using Noise and Vpeak it is possible to calculate the SNR by equation (54) and its measurement unit is decibels[42, p. 147]:

$$SNR = k * 20log_{10}^{(Vpeak/Noise)} \quad (54)$$

k is a constant equal to 1.25 that is applied to compensate for the bias in the noise estimation process.

The received range measurement signals with SNR higher than 24 dB are confirmed to be applied in the localization algorithms.

Networking

Networking provides a network among several P440 devices. In this application, P440 provides possibility of applying range measurement data among all of the devices in the network or assume some of them as reference nodes which have a specific locations that are also called anchors (anchor is the unit which does not initiate range request and just responses to the range request), and the rest as mobile nodes which we can calculate their locations based on their distances from the anchors. The reference nodes should be configured as an anchor to decrease the network traffic and collision among data packets. P440 supports both types of networking that are ALOHA and TDMA. In this case, all of the devices must have the same PII and operate in the same code channel; otherwise, failure in communication will appear[38], [42], [44].

The ALOHA protocol is modified for P440 and has some features to improve its performance. As it is described before, the ALOHA network is a random access network. There is no plan or order to manage network devices communication. Moreover, both the requester and the responder initiate a conversation without checking the network whether it is free or not. In order to decline collision in data transmission among devices in the network, TimeDomain has introduced a new feature which let the user specify the maximum and minimum interval time

in millisecond between the data transmissions. If the minimum and maximum of the interval time are equal, the unit initiates transmission in a fixed period. Another option in order to prevent a collision is Automatic Congestion Control (ACC). If the user activates ACC, The RangeNet network framework on the device will manage the ranging rate automatically based on the number of nodes in the network, the mean rate of the range requests and the duration of a conversation in the P440. Yet, ALOHA protocol has some pros and cons. The most important advantage of this protocol is that it operates via no map, order list, time slot or Slotmap to manage the communication based on that. Thus, any P440 device which has the same configuration such as the other devices in the network could join the network during the operation or leave it with no authorization. On the other hand, due to the data packets' collision, the ranging rate is very low which lead to lower localization performance[38], [44], [45].

To set up a network based on the TDMA protocol, at first, a Slotmap should be defined. Slotmap contains several slots and each slot specifies which of the P440 devices is allowed to request from which device in the network by a specific PII and in a specific time in each cycle via which code channel. Each slot contains Requester Node ID, Responder Node ID, PII, Code Channel, Antenna mode, request data, response data and the data type of communication (range or data). The maximum number of slots in a Slotmap is 32 till now, but the manufacturer attempts to raise it to 64 in the next Range net update. The configuration of the Slotmap should be the same in all of the P440 devices in the network; if not, it makes asynchronous data transmission which led to lower performance[38], [45].

Positioning

P440 has a Location Operation mode (location engine) which receives the range measurements and derives the location in X, Y and Z dimensions in its own frame. The mobile node takes advantage of the networking and shares the location information with the entire devices thus the end-user can connect to one of the devices in the network and receives the location data. In order to have a location in 2D, at least 3 reference nodes or anchors are required and as in 3D, 4 anchors. The Location Operation mode has 3 different modes:

1. Idle: In this mode, the Mobile node and Anchors communicate with each other without any ranging or location calculation.
2. Autosurvey: this mode operates by 3 or 4 anchors and discovers the locations of the anchors automatically to build the Location Map more accurately, though it is inoperable for more than 4 anchors. To execute this operation mode, all the anchors must have LOS to each other.
3. Tracking: In this mode, the mobile device receives range data from anchors and calculates its location and shares the location data in the network.

ALOHA and TDMA (Slotmap and Auto) are two types of the network which support the Location Operation mode. The TDMA Slotmap employs the Slotmap in the Ranging and Networking while the Auto builds an internal Slotmap based on the Location Map and performance of the TDMA Auto is higher than TDMA Slotmap. The Location Operation mode (location engine) works with 2 solvers:

1. Geometric Solver: this type of solver is more appropriate to the stationary or slow-moving mobile nodes and via Nonlinear Least Square method calculates the location.
2. Kalman Solver: this solver calculates the location via range data and a motion model.
3. In order to operate in Location Operation mode, a Location Map is required. Location Map consists of all of the devices which are used in localization by Node ID and their roles in the localization such as Mobile node, Anchor node, Origin, -/+X-Axis, -/+Y-Axis or Z-Axis and the nodes' coordinates. The location engine calculates the X, Y and Z location, the variance of the X, Y and Z and also the covariance of the XY, XZ and YZ[45, p. 86]. In Figure 13, a small Cartesian coordinate system is shown.

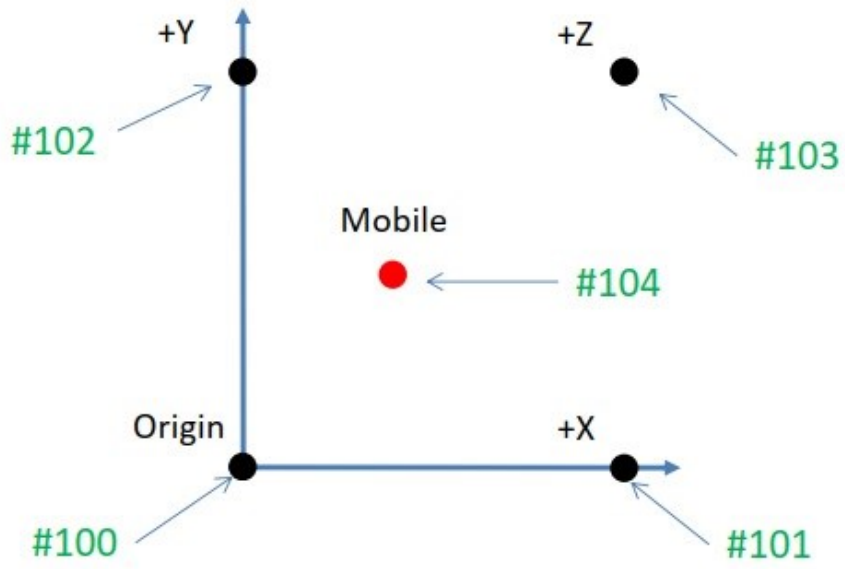

Figure 13. *Cartesian Coordinate system with Origin, +X, +Y and Z Anchors and one Mobile node*[45, Figs. 11–7]

An important point about coordinates of the anchors is the Z of the coordinates should be equal or higher than 2 meters.

3. METHODOLOGY

Methodology is commonly known as a plan to solve a problem and consists of numerous specific elements such as models, techniques, tools, different tasks and various phases[46]. This chapter is dedicated to the presentation of the model, technologies, and tools which are employed in the implementation of the proposed solution in order to achieve a stable indoor and outdoor localization regarding GNSS and UWB sensors. Furthermore, the model of the proposed solution is described to have a more comprehensive description.

3.1 Model

The model is an abstraction of the required features of the real world such as mathematical, physical and graphical features[47]. Moreover, the model should be defined in a way that fulfills all the demanded conditions. Unified Modeling Language (UML) is one of the standard notations that is used to demonstrate this model. The model in this thesis includes all the functions and algorithms that are presented in Figure 14 via UML sequence diagram.

Figure 14 reveals that the model consists of a few sensors such as GNSS, UWB, IMU and velocity (odometer) and several function blocks such as Trilateration, EKF on Trilateration location, EKF on Range, EKF on GNSS and Body pose. In the following, function blocks are described in brief.

Trilateration function block starts to receive range data of the UWB sensor and saves the ranges data of the UWB sensor with respect to the anchors in a matrix. Then, by employing trilateration algorithm on the most recent 3 ranges data from 3 various anchors which their timestamps are not older than 300 ms, the location is calculated. In order to validate the location data, Time Stamp, Solvability or Range Examination methods (will be described in the next chapter) are applied. Moreover, this function generates the variance of the calculated location which is described formerly. The location data and its variances are sent persistently to the EKF on Trilateration location and EKF on Range function blocks to be employed as their initialization location data and as the measured value in the EKF on Trilateration location function block.

EKF on Trilateration location function block implements the EKF on the location data which is generated by Trilateration function block and it is described in detail in the next chapter. The inputs of this block are generated location data by Trilateration function block, angular velocity with respect to the axis Z of the Body frame $\{B\}$, yaw of the GNSS only in the initialization step and velocity in direction of axis X of the Body frame $\{B\}$.The calculated location data of this function block is forwarded to the Body pose function block.

EKF on Range function block applies EKF on the range data between UWB mobile device and each anchor. The relative states of the EKF are initialized via location data which is generated by the Trilateration function block. The inputs of this function block are identical as EKF on Trilateration location function block in addition to the range data which is received directly from UWB mobile device. The output of this function is also location data which is forwarded to the Body pose function block.

EKF on GNSS implements the EKF on the GNSS data and the inputs come from GNSS, IMU and velocity sensors. The generated location data of this function is directed to the Body pose function block.

Body pose function block receives the generated location data of the EKF on Range, EKF on Trilateration location and EKF on GNSS function blocks. This function block receives the first 300 valid GNSS location data variances and calculates the mean of them. Then, it compares the next GNSS location data variances with the calculated mean value. If the new variance values are more than 15% of the mean value, it switches the output location data to the location data of the EKF on Range and EKF on Trilateration location function blocks.

3.2 Technologies and tools

The technologies and tools are the collection of the software, Integrated Development Environments (IDEs) and code generators which are used to build the models and other elements. They should support the required features of the techniques and models.

In this thesis, various technologies and tools such as MATLAB, Python and MATLAB Simulink were tried. The main reason of tool substitution is providing the requirements of the real-time model that is not only supporting the capability

of swift mathematical computation but also high performance in network communication to prevent data frame loss.

3.2.1 MATLAB

MATLAB is a high-level programming platform which is based on the MATLAB programming language and a matrix-based programming language and makes it possible to articulate complex mathematics in the simplest means. More information regarding MATLAB can be found in[48].

MATLAB is a powerful tool in computational mathematics and matrix algebra, however, the performance of the computational rate in implementing a real-time model is not satisfying. Therefore, MATLAB is not a proper tool in our case.

3.2.2 Python

Python is a high level and open source programming language. Developers mostly take advantages of Object-Oriented, interpretation and dynamic semantic features of Python. More information about Python is presented in[49].

Python is a high potential and flexible programming language from development point of view and also easy to debug and test due to its strong debugger while it is not as powerful and prompt as MATLAB in computational mathematics and matrix-based calculations. Thus Python does not provide the requirements of a real-time model.

3.2.3 MATLAB Simulink

MATLAB Simulink real-time is a product of MathWorks supporting Simulink models with slight restriction in employing complicated functions on the dedicated computer hardware. More information regarding MATLAB Simulink real-time could be found in[50].

MATLAB Simulink real-time provides the entire requirements of a real-time model such as computational time in almost $1ms$ and stable network communication with sensors preventing loss of data packages. Furthermore, building and generating a real-time model which should be stored and executed on the Simulink real-time PC. Finally, MATLAB Simulink real-time is selected due to the provided features.

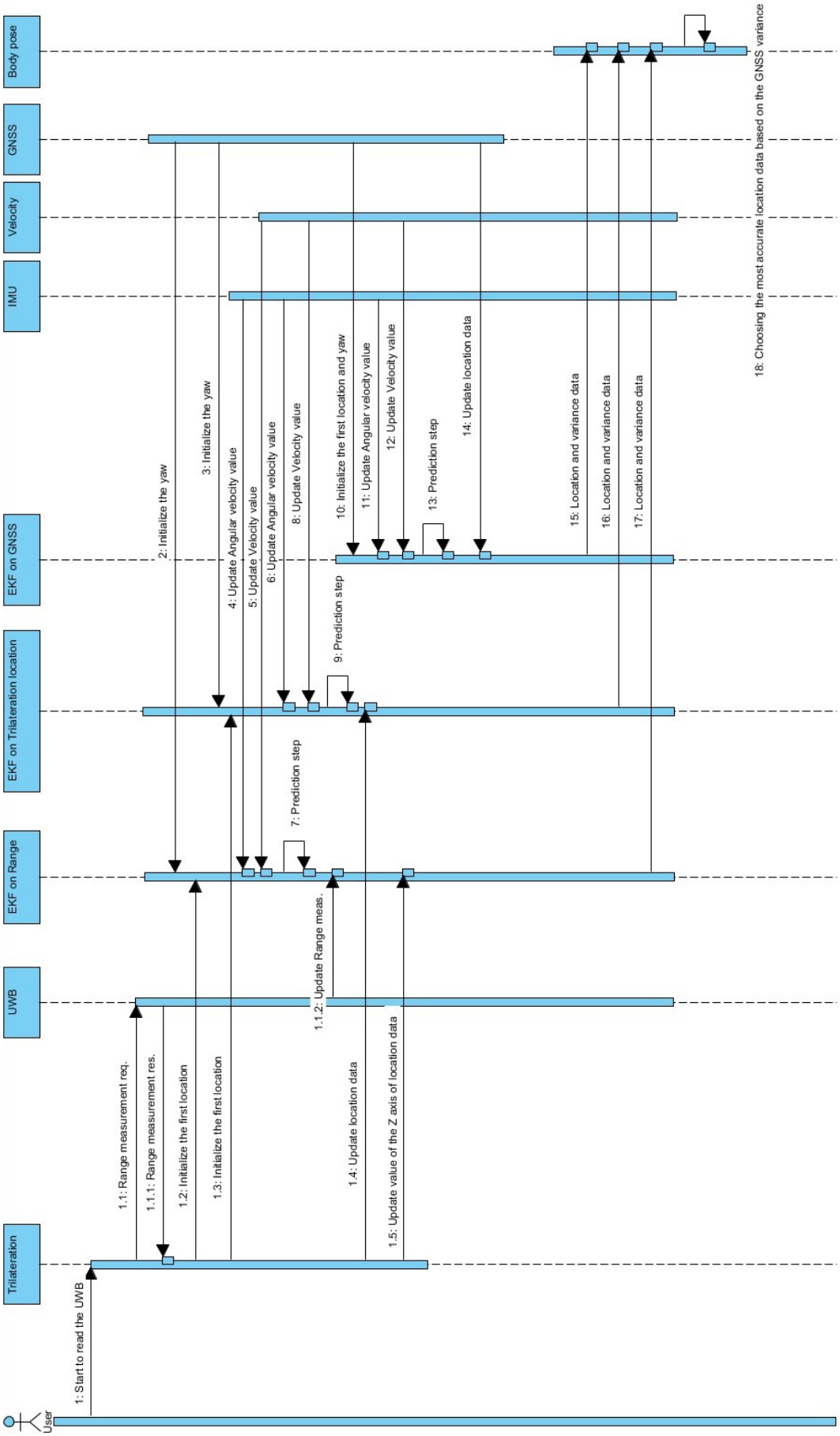

Figure 14. *UML Sequence diagram of the model*

4. LOCALIZATION EXECUTION

This chapter is dedicated to the implementation of the Body frame localization. At first, there is a description regarding the Location mode application of P440 and the relative results of the experiment followed by implementation of both geometric and EKF localization on the calculated locations of Trilateration function block and on the range data, then a comparison of the results and finally a short analysis on the environment are presented.

4.1 Location mode

This subchapter discusses the Location Operation mode of the P440 that is based on the P440 location engine.

At first, it was supposed to receive the location data from P440 instead of the range measurement data. But by the following experiment, the device reveals that if the Mobile node has no LOS to one of the references (any type of anchors: Origin, -/+X-Axis, -/+Y-Axis or Z-Axis or anchors), it stops the generation of location data or generates with a large time gap.

4.1.1 Calibration in Location mode

The experiment environment is a rectangle room with 2-side windows and $97\ m^2$ area. In this experiment, 6 units of P440 are employed and each one is installed on a tripod with $2\ m$ height. 5 of the modules are used as references and 1 as a Mobile node. Node IDs 100 to 103 are applied as Origin, +X Axis, +Y Axis, Z Axis, node ID 105 as an Anchor and the mobile node is node ID 104. The coordinate of the references are gained through measuring their distances to the Origin node by a measurement tape and those are presented in Table 4.

Node ID	Type of node	X (m)	Y (m)	Z (m)
100	Origin	0.00	0.00	2.00
101	+X Axis	9.03	0.00	2.00
102	+Y Axis	-0.04	5.13	2.00
103	Z Axis	9.09	5.10	2.00
104	Mobile	4.50	2.70	0.79
105	Anchor	2.40	2.40	2.00

Table 4. *Coordinate and type of nodes in the location generation mode*

4.1.2 Location mode experiment and result

The objective of this experiment is discovering restrictions of the P440 location mode functionality in the situation that the Mobile node has NLOS with one of the references due to some sever obstacle such as a concrete wall to simulate a situation which is unavoidable in industrial situations. As it is shown in Figure 15, the green circles are the reference nodes and the dark blue circle is the Mobile node that are described in Table 4. Figure 15 is captured from the demo application of the TimeDomain Company.

In this situation, the Mobile node has NLOS to the node ID 102 which is defined as +Y Axis reference node. The mobile node has LOS with the entire reference nodes except node ID 102 and according to the manufacturer claim, 4 reference nodes are sufficient to generate the location data[45].

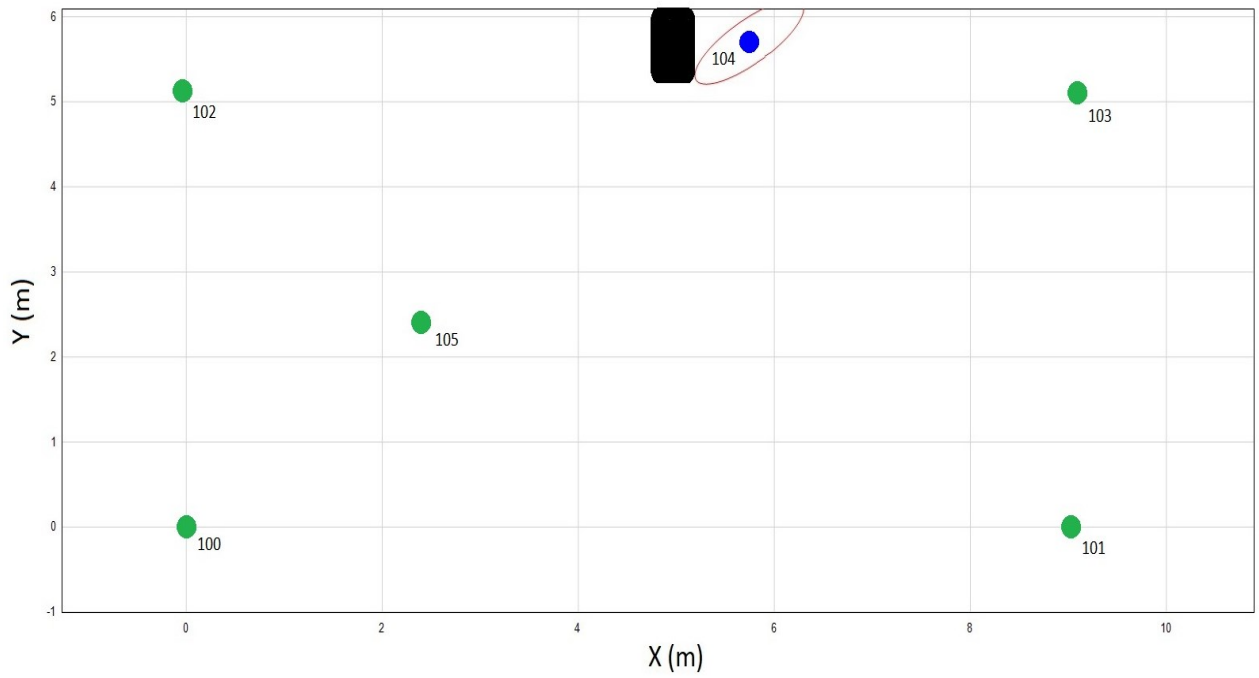

Figure 15. *Location map of the location mode experiment*

Obviously, the number of generated location data is very low as Figure 16 reveals. In this case, the PII is equal to 7 and it means that the Mobile sensor should generate location data by rate 21Hz.

As Figure 16 presents, there are various moments that the Mobile node stops location generation data specifically between a bit earlier than 200 second and after 450 second. Since there is no location data during localization for such long

time, uncertainty will dramatically grow and consequently, the accuracy will decline. Thus, the location mode of the P440 sensor seems unreliable and it is comprehensible to refuse this mode of P440 and substitute it with other localization methods such as geometric or EKF.

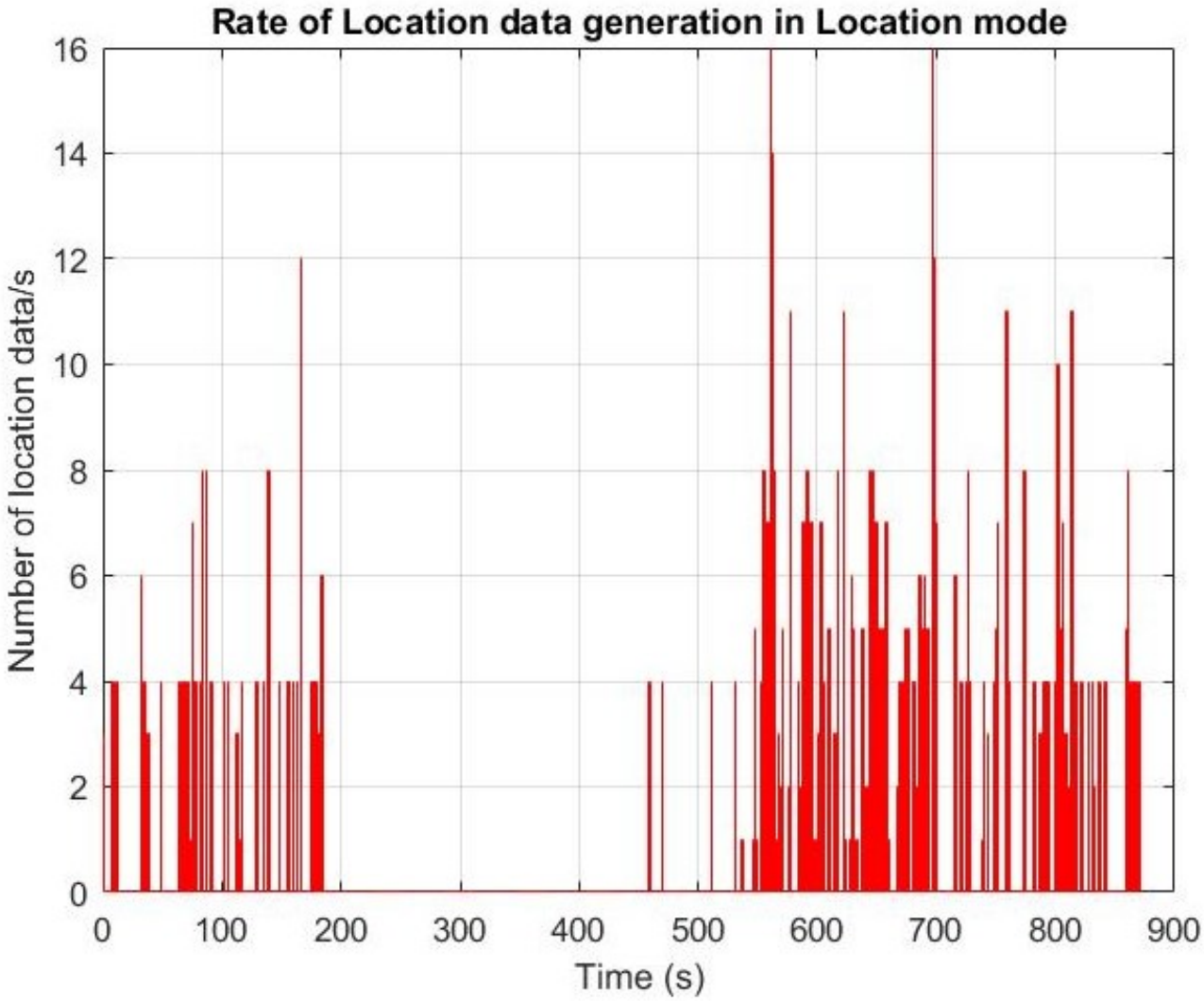

Figure 16. *Number of generated location per second*

4.2 Calibration in Ranging Network

In order to implement the localization based on the Geometric methods or EKF, a map of the reference nodes is required. This map should be integrated to the Inertial frame $\{I\}$ whose origin is somewhere near the test area. The experimental wheel loader of Tampere University Body frame $\{B\}$, GNSS, UWB, and IMU frames are in the Inertial frame. The relatives among the entire coordination system of the sensors and Body $\{B\}$ (experimental wheel loader of Tampere University) and Inertial frame $\{I\}$ are shown in Figure 17.

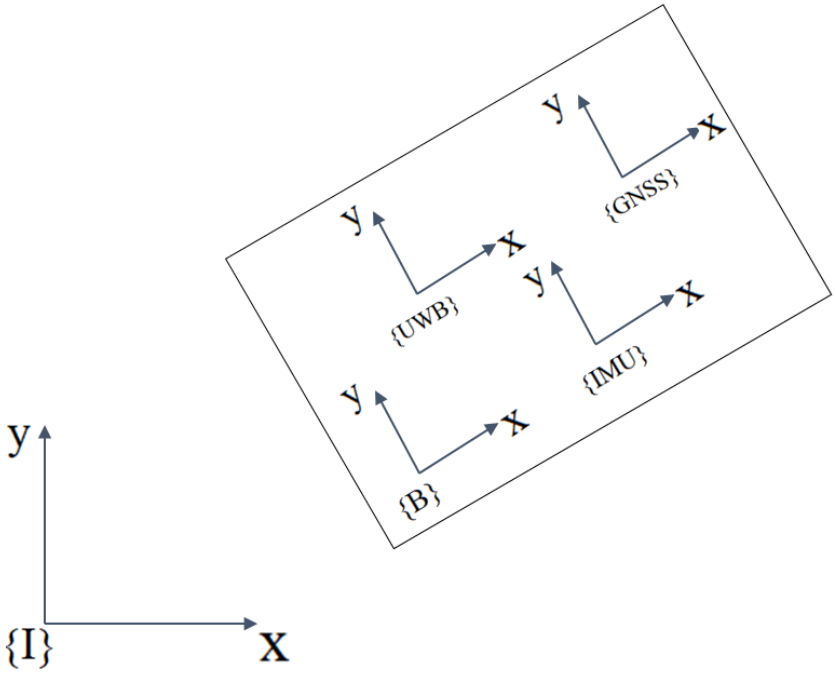

Figure 17. *The coordinate system of the sensors*

reference nodes are set up around the test area on an aluminum basement which sticks to a wooden column that is shown in Figure 18. The height of the Anchors is at least 2.45 m from the ground for the entire anchors, while the height of the ground for each anchor is different.

The GNSS location data is employed to gain the coordinate of the anchors in the inertial frame $\{I\}$ and implement the calibration of the anchors in the test area. The hall in the test area is equipped with 2 anchors which their coordinates are calculated by the trilateration method based on the relative outside anchors.

4.3 Geometric method (Trilateration)

Most of the geometric methods in UWB localization in 3 Dimensional environments that are based on 4 reference nodes while they could be more optimized to use 3 reference nodes. In order to implement Trilateration method, the algorithm of Norrdine et al.[51] is preferred due to the less number of required references and also it does not follow an iteration method which leads to a faster process. This method was mentioned previously.

As a result of equation (36), the outputs of the trilateration method contain 2 coordinates and the point is which one should be selected. A solution to this problem is applying equation (35) (Solvability method) and computing the difference

for each point. If the difference is equal to zero, that point is valid. The result of this validation method can be seen in Figure 19.

Figure 18. *Installation of a reference node around the test area*

To implement this method a matrix of the reference ID, range measurements, SNR, and the timestamp is required as it is presented in Table 5. Generally, it is called window sampling table and the trilateration algorithm does not consider the range measurements older than $300\ ms$.

Figure 19 represents the path of the localization via geometric method through the Hall and open environment in the test area. As Figure 19 reveals, there are some undesired points which are generated by the Trilateration algorithm despite of applying a validation method that is mentioned by Norrdine et al.[51] and it is called Solvability method in this research.

Node ID	Range	SNR	Time Stamp
103	25.109	44.51163	2900936
101	28.928	38.68885	2900887
103	25.106	43.84792	2900718
101	28.928	38.55565	2900669
100	20.805	40.29921	2900645
103	25.107	44.01957	2900500
101	28.928	38.75179	2900451
100	20.844	40.03409	2900427

Table 5. *An example of the window sampling table*

There is also another approach which is derived from the Data Association concept. Data Association detects the fittest anchor from a map on each measurement through a measurement model where the source of the measured range is not clear while in our case the range data senders (anchors) are identified in each data frame.

The measurement model calculates the range between the location of the relative anchor in the data frame and the calculated location of the mobile device based on the trilateration method. In the next step, the measured range will be subtracted from the calculated range by measurement model that is called the error between the measured range data and the distance between the trilateration calculated point and the anchor. The best result will be achieved when the error is almost zero. In this case, just the calculated points are accepted which their errors are less than $rangErr^2\ m.\ rangErr$ denotes to the amount of range measurement error which is provided by the sensor. The equations and notations are as equation (24) and the only difference is that the (x_N, y_N, z_N) are supposed to be calculated in equation (24) while in equation (55) those are calculated via trilateration algorithm and if the conditions of equation (55) are met, the new location data will be validated and forwarded to the EKF on Range data and EKF on Trilateration location data function blocks.

$$\begin{cases} |(x_{p1}-x_N)^2+(y_{p1}-y_N)^2+(z_{p1}-z_N)^2-s_1^2| = rangErr^2 \\ |(x_{p2}-x_N)^2+(y_{p2}-y_N)^2+(z_{p2}-z_N)^2-s_2^2| = rangErr^2 \\ |(x_{p3}-x_N)^2+(y_{p3}-y_N)^2+(z_{p3}-z_N)^2-s_3^2| = rangErr^2 \end{cases} \quad (55)$$

This approach is called Range Examination in this study and the implementation result is presented in Figure 20. Obviously, the number of the undesired points experienced a rise and that means more uncertainty and less accuracy.

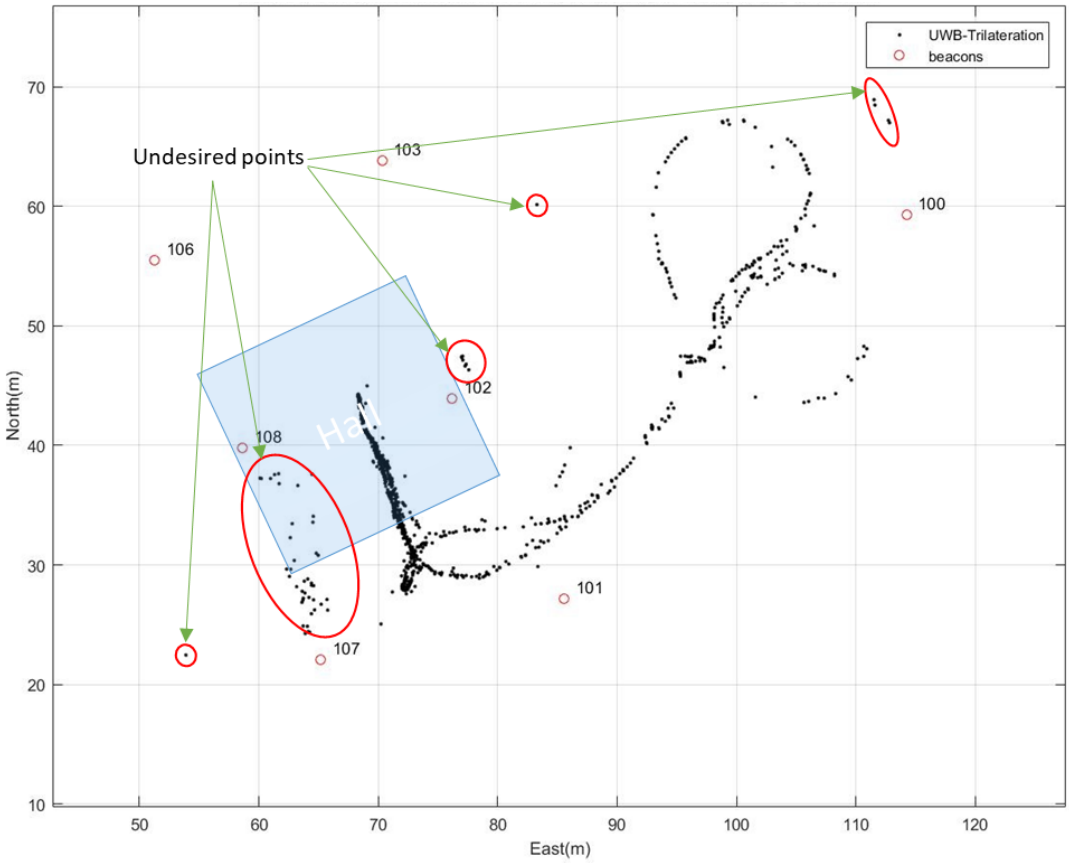

Figure 19. *Body Localization by Trilateration method within the Hall and outdoor via Solvability method*

In order to have less undesired positions, the Trilateration method results could be validated by employing the velocity of the experimental wheel loader of Tampere University and the timestamp of each calculated position. This method is based on the distance computation between the latest validated point and the new generated one via Trilateration algorithm as it is shown in equation (56) and is called TimeStamp in this study. If this condition is met, the latest calculated position will be accepted.

$$v_x * ts - ((x_t - x_{t-1})^2 + (y_t - y_{t-1})^2 + (z_t - z_{t-1})^2)^{\frac{1}{2}} = 0 \quad (56)$$

$\{x_t, y_t, z_t\}$ – Coordinates of the new position at the Inertial frame $\{I\}$

$\{x_{t-1}, y_{t-1}, z_{t-1}\}$ – Coordinates of the previous position at the Inertial frame $\{I\}$

$\{v_x\}$ – Linear velocity in the direction of x of the body frame $\{B\}$ at $\{B\}$

$\{ts\}$ – The difference between the previous and new timestamp

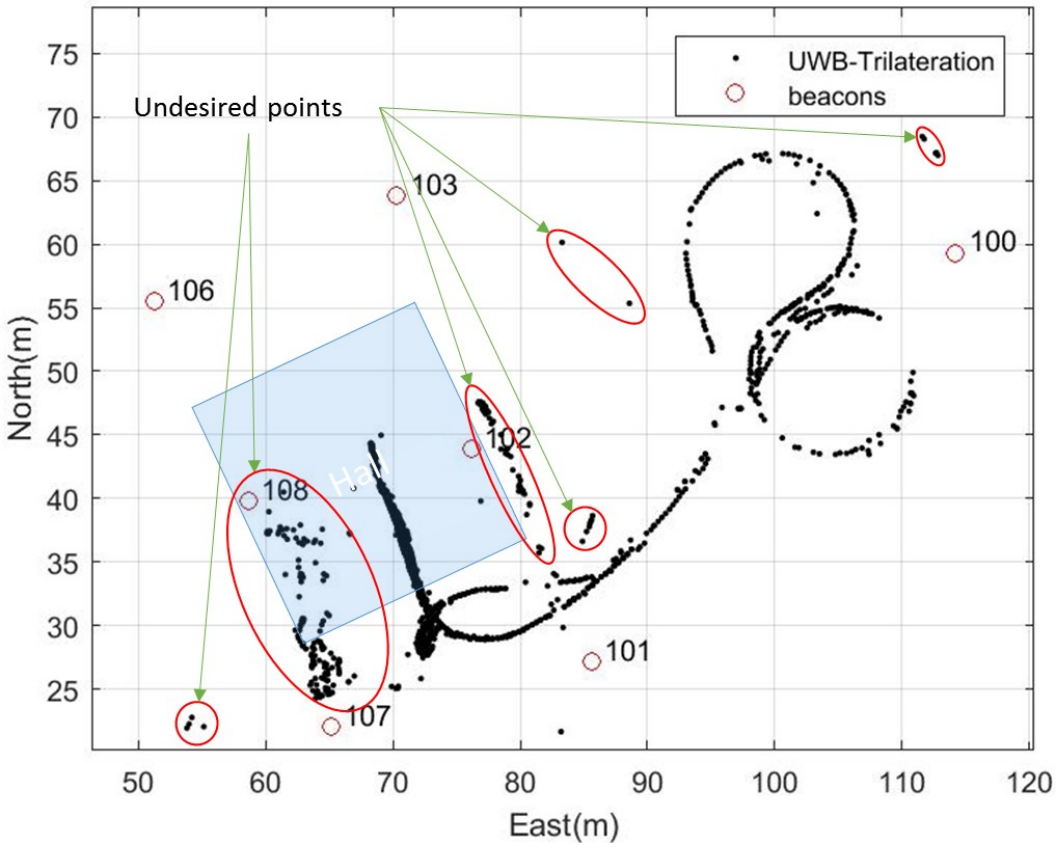

Figure 20. *Body Localization by Trilateration method within the Hall and outdoor via Range Examination method*

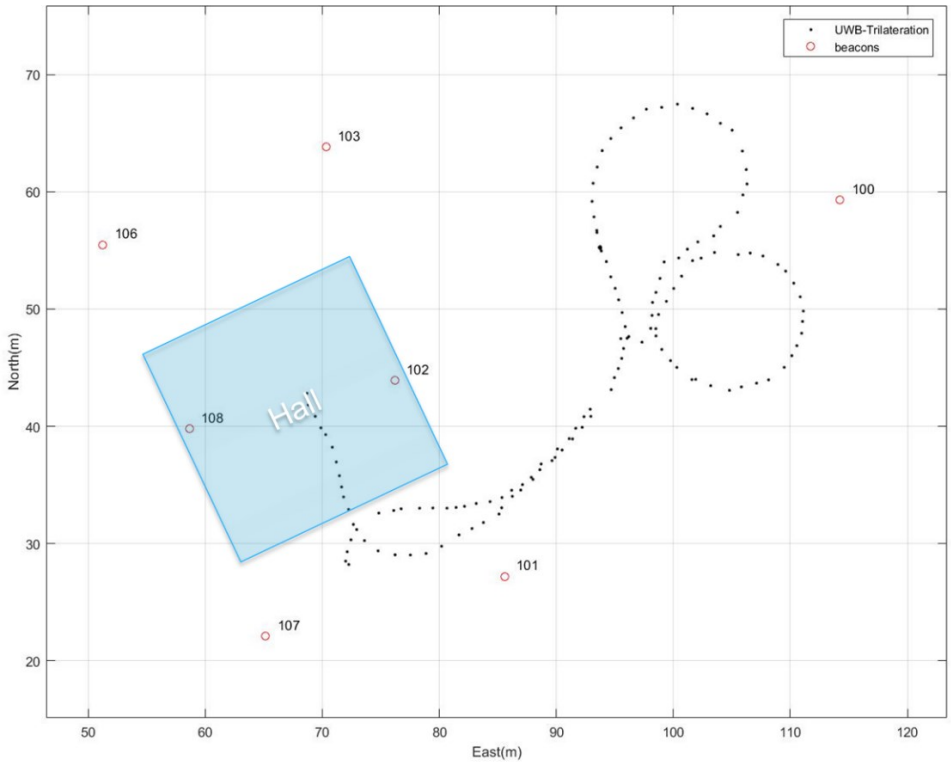

Figure 21. *Body Localization by Trilateration method within the Hall and outdoor via TimeStamp method*

Figure 21 reveals the effect of the TimeStamp data validation method. Manifestly, the number of validated positions by this method dramatically dropped.

However, the most accurate validation method of the location data generated via Trilateration method is TimeStamp method despite of the lower number of confirmed points in comparison with other methods.

The algorithm of Trilateration method, in brief, is in the following:

1: At least receiving 3 range measurements from various reference node ID (from a window timing table such as Table 5)
while (number of range measurements are less than 3 from 3 different anchors and the difference between the timestamp of the latest and the older range measurement is less than $300\ ms$)
store the row number of selected anchors
end while

2: **Implementing trilateration equations**
(26), (27), (28), (29), (30), (31), (32), (33), (34),

3: **Position calculation** by (36)

4: **validation of N_1 and N_2** by (35) or (55) or (56)

Totally, trilateration is not a proper method in localization due to the following reasons. Trilateration method is designed in order to find a point on the stationary or static situations and it does not support the effects of velocities in different directions. Thus the result is less accurate. Moreover, trilateration algorithm requires at least 3 different reference nodes range measurements. As it is shown in Table 5, from the first row of data to the 5th row which the 3 different needed reference nodes which met the $300\ ms$ condition are located. If there are some invalid range measurements based on the range data and its parameter, the difference between the timestamps will grow. In this case, the time between the latest and the older range measurement is $291\ ms$. It means for example by a velocity of $2\ m/s$ the movement of the machine between the first and the third applied range measurements is $0.582\ m$ which dramatically reduces the accuracy. Thus this method should ideally be employed only in stationary situations.

4.4 Extended Kalman Filter on the trilateration results

In order to have a smooth localization with fewer jumps on generated locations of the trilateration method, implementing EKF seems a proper choice. Based on the description of the EKF in the previous chapter, a state vector, a motion model and a measurement model are required. Therefore, a few variables will be added to the EKF notation of the previous chapter:

$\{\widehat{\ }\}$ – Hat means predicted value. When there is a hat over a variable, it means that is a predicted value of the variable.

$\{x_t\},\{y_t\},\{\psi_t\}$ – Pose of the body frame $\{B\}$ with respect to the Inertial frame $\{I\}$.

$\{b1\}$ – Denotes a time-correlated white noise of gyro bias. It is not a state but considered as a state and applied as a bias of gyro on ω_z to decrease the white noise by subtracting from ω_z and its value convergence to almost zero ($10^{-7}\ to\ 10^{-4}$). Its value is calculated based on the variance of the ω_z which is gained from gyro characteristics that is also applied in the process noise covariance matrix $\{Q_k\}$.

$\{v_x\}$ – Means linear velocity in the direction of x of the body frame $\{B\}$ at $\{B\}$.

$\{\omega_z\}$ – Means angular velocity of the gyro on the experimental wheel loader of Tampere University about an axis z of the body frame $\{B\}$.

$\{[\epsilon_{vx},\epsilon_{\omega z}]^T\}$ – Denotes control noise of velocity and angular velocity around the z-axis.

$\{r,p\}$ – Mean Roll and Pitch.

$\{\ ^IP_{UWB}\}$ – Denotes coordinate of the UWB in the Inertial frame $\{I\}$ and consists of $[x_{UWB},y_{UWB}]^T$.

$\{\ ^BP_{UWB}\}$ – Denotes coordinate of the UWB in the $\{B\}$ and consists of $[a,b,c]^T$ which are respectively the coordinates of the UWB in direction of x , y and z axes in the body frame $\{B\}$ and it is equal to $\left[\ ^Bx_{UWB},\ ^By_{UWB},\ ^Bz_{UWB}\right]^T$.

$\{\ ^IP_B\}$ – Position of the body frame $\{B\}$ in the Inertial frame $\{I\}$ and consists of $[x_t,y_t]^T$.

$\{{}^I_BR\}$ – Rotation matrix.

$\{x_0(+)\}$ – Initial value of the state vector.

$\{P_0(+)\}$ – Initial value of the state covariance.

$\{var_{uwb_X}, var_{uwb_Y}\}$ – UWB location variance which comes from trilateration function block.

4.4.1 State vector and Motion model

The state vector consists of states which are predicted and passed the update step if there is a true value for external data resources. The state vector $\{x_k\}$ and the control vector $\{u_k\}$ are presented in equation (57). The control vector contains a number of control variables such as velocity and angular velocity. The control vector is employed in the calculation of the motion model. The motion model is a set of the equations which are applied to predict the states of the state vector which is defined in the following equation (58).

$$x_k = \begin{bmatrix} x_t \\ y_t \\ \psi_t \\ b1 \end{bmatrix}, \qquad u_k = \begin{bmatrix} v_x \\ \omega_z \end{bmatrix} + \epsilon, \qquad \epsilon = \begin{bmatrix} \epsilon_{vx} \\ \epsilon_{\omega z} \end{bmatrix} \tag{57}$$

$$\hat{x}_k(-) = \phi_{k-1}(x_{k-1}(+), u_k), \phi_{k-1} = \begin{bmatrix} x_{t-1} \\ y_{t-1} \\ \psi_{t-1} \\ b1 \end{bmatrix} + \begin{bmatrix} ts * v_x * cos\,\psi_{t-1} * \cos p \\ ts * v_x * sin\,\psi_{t-1} * \cos p \\ ts * \dfrac{\cos r * (\omega_z - b1)}{\cos p} \\ -b1 * ts/\boldsymbol{\tau} \end{bmatrix} \tag{58}$$

4.4.2 Measurement model

The measured values could be modeled by equation (44). Instead of the real measured values of the position from UWB in the Inertial frame $\{I\}$, the position values are gained directly from the Trilateration function block that is given by (59):

$$z_k = {}^{I}P_{UWB} = \begin{bmatrix} x_{tri\_UWB} \\ y_{tri\_UWB} \end{bmatrix} \tag{59}$$

In our case, z_k is used in 2D and in the last step z_{tri_UWB} will be added to the location data of the body frame $\{B\}$ in the Inertial frame $\{I\}$.

Equation (60) presents the relation between ${}^{I}P_{UWB}$ and ${}^{I}P_{B}$ by using the transformation matrix ${}^{I}_{B}\hat{R}$ and the position of the UWB in the body frame $\{B\}$ ${}^{B}P_{UWB}$.

$${}^{I}P_{UWB} = {}^{I}P_{B} + {}^{I}_{B}\hat{R} \times {}^{B}P_{UWB} \tag{60}$$

With the aim of predicting the measurement, the equation (60) can be employed such as equation (61). The only value of the location of the body in the ${}^{I}P_{B}$ is predicted value and the result which is ${}^{I}\hat{P}_{UWB}$, is also a predicted value for the measurement.

$$ {}^{I}\hat{P}_{UWB} = {}^{I}\hat{P}_{B} + {}^{I}_{B}\hat{R} \times {}^{B}P_{UWB} \tag{61} $$

Where the rotation matrix ${}^{I}_{B}\hat{R}$ can be computed based on the orientation of experimental wheel loader of Tampere University around axis z of the Body frame $\{B\}$ which is known as yaw ψ_t, like equation (63). In our notation, the rotation matrix always is applied as the predicted value ${}^{I}_{B}\hat{R}$ because it is always a prediction. ${}^{B}P_{UWB}$ is the location of the UWB in the body frame $\{B\}$ in a 3D environment like as $[a\ b\ c]^T$ but due to the problem in having roll and pitch, it will be applied like the format which is mentioned in the equation (63). In equation (60), the assumption is the ${}^{I}P_{UWB}$ is such as equation (62) due to the calculation of the roll and pitch faces problem and it is not possible to predict z_{UWB} since in the prediction of z_{UWB} the pitch is required, but when the z_{UWB} is required in any next steps of the calculation, it is possible to apply the z_{UWB} which is received directly from the trilateration method after transforming to the body frame $\{B\}$ with respect to the $\{I\}$:

$$ z_k = {}^{I}P_{UWB} = \begin{bmatrix} x_{UWB} \\ y_{UWB} \end{bmatrix} \tag{62} $$

$$ {}^{I}_{B}\hat{R} = \begin{bmatrix} \cos\hat{\psi}_t & -\sin\hat{\psi}_t \\ \sin\hat{\psi}_t & \cos\hat{\psi}_t \end{bmatrix}, \quad {}^{B}P_{UWB} = \begin{bmatrix} a \\ b \end{bmatrix}, \quad {}^{I}\hat{P}_{B} = \begin{bmatrix} \hat{x}_t \\ \hat{y}_t \end{bmatrix} \tag{63} $$

Thus, the measurement model can be (64).

$$ \hat{z}_k = h\big(\hat{x}_k(-)\big) = \begin{bmatrix} \hat{x}_t + a * \cos\hat{\psi}_t - b * \sin\hat{\psi}_t \\ \hat{y}_t + a * \sin\hat{\psi}_t + b * \cos\hat{\psi}_t \end{bmatrix} \tag{64} $$

4.4.3 Prediction step

In the prediction step, the state vector and the covariance matrix should be predicted. Equation (58) is responsible for the prediction of the state vector. In order to predict the covariance matrix, the Φ_{k-1} and L_c are required to be defined. The both are defined based on the equations (47) and (48) which are Jacobians

of the motion model with respect to the state vector and control noise, respectively, as they are shown in the following equations (65) and (66).

$$\Phi_{k-1} = \begin{bmatrix} 1 & 0 & -ts * v_x * \sin\psi_{t-1} * \cos p & 0 \\ 0 & 1 & ts * v_x * \cos\psi_{t-1} * \cos p & 0 \\ 0 & 0 & 1 & -ts * \dfrac{\cos r}{\cos p} \\ 0 & 0 & 0 & 1 - \dfrac{ts}{\tau} \end{bmatrix} \tag{65}$$

$$L_c = \frac{\partial \phi_k}{\partial \epsilon}|_{\epsilon=0} = \begin{bmatrix} \cos\psi_{t-1} * \cos p & 0 \\ \sin\psi_{t-1} * \cos p & 0 \\ 0 & \dfrac{\cos r}{\cos p} \\ 0 & 0 \end{bmatrix} \tag{66}$$

To calculate Q_k, it is necessary to have the covariance matrix of the control vector which consists of $\{v_x, \omega_z\}$ and also to linearize the control noise that is presented with $\{L_c\}$ which is Jacobian of the motion model with respect to the Control noise vector $\{\epsilon\}$. The covariance matrix includes the variance of each control factor in its main diagonal.

$$Q_c = 10^{-4} * \begin{bmatrix} 1.0 & 0 \\ 0 & 0.0001 \end{bmatrix} \tag{67}$$

The process noise Q_k is calculated in equation (68):

$$Q_{k-1} = L_c * Q_c * L_c^T \tag{68}$$

Finally, the required variables to predict the covariance are available and the prediction is shown in equation (69):

$$P_k(-) = \Phi_{k-1} P_{k-1}(+) \Phi_{k-1}^{\mathrm{T}} + Q_{k-1} \tag{69}$$

The prediction could be performed whenever a new value from odometer received.

4.4.4 Initialization of the State vector and Covariance matrix

The state vector requires to be initialized based on the values received from the trilateration method for $\{x_t\}$ and $\{y_t\}$. in order to Initialize yaw $\{\psi_t\}$, the first validated received value of the yaw from GNSS is employed, then the value of the $\{\psi_t\}$ will just be anticipated by the odometry method without no more using

yaw of the GNSS. Initialization of the yaw $\{\psi_t\}$ must be based on the GNSS yaw because the UWB localization as a complementary of the GNSS localization is supposed to be substituted where the GNSS localization is not valid. Therefore, the UWB localization is independent of GNSS localization except in the initialization of the yaw $\{\psi_t\}$ that is unavoidable. Equation (71) represents the initialization of the state vector after transformation from UWB frame $\{UWB\}$ to the body frame $\{B\}$ (equation (70)).

$$ {}^{I}P_B = \begin{bmatrix} x_t \\ y_t \end{bmatrix} = {}^{I}P_{UWB} - {}^{I}_{B}R * {}^{B}P_{UWB} \tag{70} $$

$$ x_0(+) = \begin{bmatrix} x_t \\ y_t \\ \psi_t \\ b1 \end{bmatrix} = \begin{bmatrix} x_t \\ y_t \\ \psi_{GNSS} \\ 0 \end{bmatrix} \tag{71} $$

In order to initialize the covariance matrix of the state vector, the values of the main diagonal should be assigned based on the initial uncertainty of the states. In this case, the uncertainty of initial values of $\{x_t\}$ and $\{y_t\}$ are related to the variance values of $\{x_t\}$ and $\{y_t\}$ (var_{uwb_X},var_{uwb_Y}) which come from trilateration function block and are related to the location estimation. Plus, yaw $\{\psi_t\}$ and $\{b1\}$ are initialized with large values on their own scale. The other indices of the covariance matrix should be zero to indicate the states are uncorrelated. Equation (72) presents the initialization of the covariance matrix.

$$ P_0(+) = \begin{bmatrix} var_{uwb_X} & 0 & 0 & 0 \\ 0 & var_{uwb_Y} & 0 & 0 \\ 0 & 0 & \frac{pi}{180} & 0 \\ 0 & 0 & 0 & 10^{-6} \end{bmatrix} \tag{72} $$

4.4.5 Update step

Update step is performed at the moment a new position data attains from trilateration function block, and the values of the state vector and covariance matrix will be updated based on the new location data. At first, the equation (50) should be expanded and defined as equation (73):

$$H_k = \frac{\partial h_k}{\partial x}|_{x=\hat{x}_k(-)} = \begin{bmatrix} 1 & 0 & -a * sin\,\hat{\psi}_t - b * cos\,\hat{\psi}_t & 0 \\ 0 & 1 & a * cos\,\hat{\psi}_t - b * sin\,\hat{\psi}_t & 0 \end{bmatrix} \quad (73)$$

The value of the measurement noise covariance matrix R_k is in the following (74):

$$R_k = \begin{bmatrix} var^2_{uwb_X} & 0 \\ 0 & var^2_{uwb_Y} \end{bmatrix} \quad (74)$$

Now it is possible to calculate the Kalman gain is succeeded as equation (75):

$$K_k = P_k(-)H_k^T(H_k P_k(-)H_k^T + R_k)^{-1} \quad (75)$$

And finally, the value update of the state vector and covariance matrix are in the ensuing, equations (76) and (77):

$$\hat{x}_k(+) = \hat{x}_k(-) + K_k(z_k - \hat{z}_k) \quad (76)$$

$$P_k(+) = (I - K_k H_k)P_k(-) \quad (77)$$

This EKF is implemented on the validated position data of the trilateration function block and the position data takes advantage of the following validation methods which are Solvability, TimeStamp or Range Examination method.

The algorithm of EKF on trilateration location data is in brief in the following:

1: Initialization of the state vector and covariance of the states (71), (72)
2: **If** new IMU, velocity data
    Do Prediction step (58), (65), (66), (67), (68), (69)
   End if
3: **If** new location data from trilateration
    Do Update step (64), (73), (74), (75), (76), (77)
   End if

This algorithm will be executed in an infinite loop.

4.5 Extended Kalman Filter on Range data

The main difference between this EKF and the previous one is in the measurement model. In the former one, the measurement model deals with the location data while in the latter one the model is modified with the range data of the mobile node with anchors. Thus the measurement model, the measurement

noise covariance matrix and a few equations which are mentioned in the next parts are modified.

As we have the same motion model as the previous EKF, the prediction of the ${}^{I}P_{B}$ should be transformed to the UWB frame $\{UWB\}$ via the previous measurement model equation (64). Hence the predicted position of the UWB ${}^{I}P_{UWB}$ in 2D is prepared but the z_t of the position is required due to the 3D range measurement. Thus the z_t will be supplied from trilateration function and be added to 2D location data of the UWB in the $\{I\}$ such as the following equation.

$$ {}^{I}P_{UWB} = \begin{bmatrix} \hat{x}_t + a * \cos\hat{\psi}_t - b * \sin\hat{\psi}_t \\ \hat{y}_t + a * \sin\hat{\psi}_t + b * \cos\hat{\psi}_t \\ z_t \end{bmatrix} \tag{78} $$

Now the location of the anchor in the Inertial frame $\{I\}$ ${}^{I}P_{anchor}$ is required to form the measurement model.

$\{m_{ix}, m_{iy}, m_{iz}\}$ – Coordinate of the anchor in the Inertial frame $\{I\}$.

$$ {}^{I}P_{anchor} = \begin{bmatrix} m_{ix} \\ m_{iy} \\ m_{iz} \end{bmatrix} \tag{79} $$

The measurement model could be such as the following equation.

$$ \hat{z}_k = h\big(\hat{x}_k(-)\big) = \| \ {}^{I}P_{UWB} - \ {}^{I}P_{anchor} \| \tag{80} $$

The Jacobian of the measurement model with respect to the state vector is presented in equation (81).

$$ \begin{gathered} A = a * \cos\hat{\psi}_t - \ b * \sin\hat{\psi}_t + \hat{x}_t - m_{ix} \\ B = a * \sin\hat{\psi}_t + \ b * \cos\hat{\psi}_t + \hat{y}_t - m_{iy} \\ H_k = \left[\frac{A}{\hat{z}_k}, \frac{B}{\hat{z}_k}, \frac{A * \left(-a * \sin\hat{\psi}_t - \ b * \cos\hat{\psi}_t\right) + B * \left(a * \cos\hat{\psi}_t - \ b * \sin\hat{\psi}_t\right)}{\hat{z}_k}, 0\right] \end{gathered} \tag{81} $$

A and **B** are just applied to have a shorter equation.

The value of the measurement noise covariance matrix is such as equation (82). The range error value is multiplied to 5 due to its very small value.

$$ R_k = (5 * rangeError)^2 \tag{82} $$

$\{rangeError\}$ – It is included in the sensor range data frame and is generated by the sensor. Moreover, its value normally varies from 0.024 to 0.055m.

The rest of this EKF is like the previous one and there is nothing new to describe.

The algorithm of EKF on the range data is in brief in the following:

1: Initialization of the state vector and covariance of the states (71), (72)
2: **If** new IMU or velocity data
    Do Prediction step (58), (65), (66), (67), (68), (69)
   End if
3: **If** new range data from UWB mobile node
    Do Update step (80), (81), (82), (75), (76), (77)
   End if

This algorithm will be repeated in an infinite loop.

4.6 Structure of the model

In Figure 22, the relation among different blocks of the model such as trilateration, EKF on trilateration location data and EKF on range data and various sensors such as UWB, GNSS, IMU, and velocity are illustrated. This relation was presented in Figure 14 with more details.

As it can be seen in Figure 22, IMU supports the three EKF function blocks by angular velocity. Velocity which is known as velocity in the x-axis direction of the Body frame $\{B\}$ and is employed in all function blocks and UWB range data is also required in the Trilateration and EKF on Range data function blocks. GNSS sensor data is required to initialize the both EKF function blocks which are implemented on the UWB data and trilateration location data.

The output of the EKF on Range data, EKF on Trilateration and EKF GNSS are inputs of the Body pose function block. At first, Body pose function block calculates an average from 300 confirmed GNSS standard deviation values of x and y to have a reference value in order to switch between location data of EKF GNSS and EKF on Range data or EKF on Trilateration. When the standard deviation of the x and y are increased more than 15% of the average value, the final location data will be switched to the location data of EKF on Range data or EKF on Trilateration from EKF GNSS and vice versa.

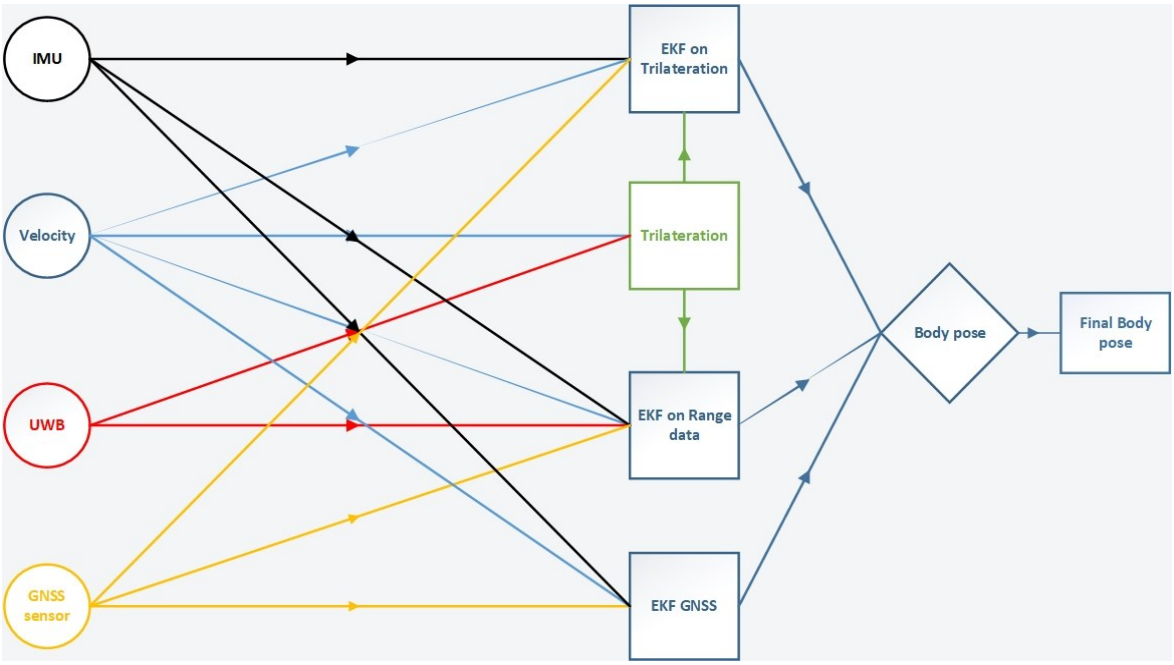

Figure 22. *Relation among Function Blocks and sensors*

The update rates of the output of the sensors are presented in Table 6. The time between receiving each measurement signal of the Odometry is exactly $20ms$ so the update rate is $50Hz$. The update rate of the UWB in TDMA mode is calculable and fixed because of the characteristics of this method, but if the UWB devices operate in ALOHA mode, the update rate entirely depends on the number of the anchors which are in the line of sight with UWB mobile node.

Sensor	Output Variables	Update rate (Hz)
IMU	Angular velocity	128.75
Odometry	Velocity	50.00
UWB	Range data	47.62

Table 6. *Sensor update rates (Hz)*

4.7 Results

In this subchapter, the results of the experiments in the 2 different environments are presented.

In the following, Table 7 presents the average and maximum difference between the EKF on Trilateration location data, EKF on Range data and EKF on GNSS data. A few figures which are related to Table 7 information, demonstrate the plot of the results of the localization by EKF on Trilateration location data and

EKF on Range data in comparison with EKF on GNSS location data. The true value in the calculation of the average and the maximum difference is the value of the EKF on GNSS when it is valid; otherwise, there is no reference value.

The importance of the data validation method of the calculated points in the output of the Trilateration method is due to the lack of the roll and pitch which were derived from the IMU problem. Based on the equation (78), (79) and (80), in order to predict the range measurement, z_t is required while due to the IMU, the roll and pitch are unavailable and the only solution to the loss of pitch is inserting the value of the z_t from Trilateration calculation which grows the inaccuracy because of its intrinsic inaccuracy which is derived from the delay in receiving the proper number of the range data.

Validation method	Environment	Average difference(m)		Maximum difference(m)	
		EKF on Range	EKF on Trilateration	EKF on Range	EKF on Trilateration
Solvability	In/Outdoor	0.0603	0.2540	0.4082	6.8491
	Outdoor	0.1803	1.1045	0.7402	7.6443
Time Stamp	In/Outdoor	0.0460	0.1204	0.2857	0.6386
	Outdoor	0.1320	0.3721	0.4643	1.1240
Range Examination	In/Outdoor	0.0632	0.2006	0.4824	6.6054
	Outdoor	0.1972	0.9235	0.8071	15.4373

Table 7. *Average and Maximum difference in Body frame localization*

The methods which are applied to filter the generated location data of Trilateration method are Solvability which is based on the difference value that is shown in the equation (36), The Time Stamp method (equation (56)) that employs the velocity of the vehicle and the difference between timestamp of the previous validated location data and the new one to validate the new generated location data and the Range Examination method (equation (55)) that refers to the Data Association approach.

The Solvability method generates a high number of location data that some of which are undesired. The Time Stamp method filters all of the undesired points; however, the number of the confirmed location data is not high, but the accuracy is higher than other approaches. The Range Examination method also eliminates

a number of the unwanted points, yet not as good as Time Stamp method. The results of these approaches are mentioned in Table 7.

In order to enhance the accuracy in the EKF on range data method, NLOS range measurements should be eliminated. P440 has the feature to eliminate the NLOS measurements while in the experiments this feature presents a low performance. Therefore, the range measurements which are different from the expected measurements of more than $30\ cm$, are ignored. This is another reason for the higher accuracy of the EKF on range data in comparison with EKF on Trilateration location data.

In Table 7, the first column contains the name of the employed validation method on the generated location data of Trilateration method. The second one presents the environment of the experiment. If the experiment is conducted both in outdoor and inside of the Hall, the in/outdoor is used else it is Outdoor. The average difference column presents the average difference of the both EKF on the range and EKF on Trilateration location data with EKF on GNSS data when it is valid. Finally, the last column (Maximum difference) has the same situation as the Average difference column, but it illustrates the maximum difference values of the both EKF on the range and EKF on Trilateration location data with EKF on GNSS location data.

Solvability is the validation method and within the hall and outdoor is the experiment environment in the first row of Table 7. Figure 23 presents all localization methods. As the figure depicts, there are red and blue dots and green line which are respectively EKF on range data, EKF on the Trilateration location data and the result of EKF on GNSS data which is the true value when it is valid. The average difference value between EKF on range data and EKF on GNSS data which is called accuracy in this study is $6.03\ cm$ while in case of the EKF on Trilateration location data the accuracy is $25.40\ cm$. Obviously, EKF on range data is more accurate than EKF on Trilateration location data. The final localization is implemented via a combination of EKF on GNSS and EKF on range data which the plot of the Body frame localization is shown in Figure 24. As it is presented in Figure 24, the jump in switching point from EKF on GNSS to EKF on range localization is almost $10.92\ cm$ while the jump point from EKF on GNSS to EKF on Trilateration location data is almost $183\ cm$ which is an inappropriate value.

As Figure 24 reveals, the localization of the Wheel Loader of Tampere University after leaving the hall to the final point continues on the EKF on range data of UWB due to a certain reason. When GNSS does not have LOS to at least 4 satellites, the generated location variances of the GNSS will be increased and after observing the minimum required number of satellites, the variances will experience a continues decline. The threshold variance value in the proposed algorithm is 15% more than the calculated average value and the return threshold variance value is the same. The mean value of the location variances at the beginning of the experiment are 0.0082, 0.0066, 0.0174 respectively in x, y and z axes while in the endpoint of the experiment the location variances are 0.0114, 0.0085 and 0.0461. Thus there are a rise of 39%, 28%, and 164% in axes x, y, and z, accordingly. By magnifying a jump point in Figure 23, unsteadiness in the localization with GNSS after leaving the Hall is shown. Therefore, the localization will be continued based on the UWB until the end of the experiment. Achieving the 15% threshold of the GNSS location data variance is experimentally and also it prevents fluctuation and over switching between GNSS and UWB data and led us to have a more stable localization.

The second row of data in Table 7 belongs to the same situation as the first row, but the difference is in the environment of the experiment that is completely outdoor. In this case, EKF on the range data has also higher accuracy. Figure 25 shows the comparison among EKF on range data (red dots), EKF on the Trilateration location data (blue dots) and EKF on GNSS (green line). The experimental wheel loader of the Tampere University is driven outdoor completely and thus the localization follows the GNSS data. Obviously, the accuracy of the EKF on range data is higher than the accuracy of the EKF on Trilateration location data and the average accuracies are $18.03\ cm$ and $110.45\ cm$, respectively. The main reason for lower accuracy on localization with trilateration location data via Solvability data validation method is the high number of the irrelevant location data which highly affects the correction factor of the EKF $(z_n - \hat{z}_n)$ and consequently, the correction factor causes wrong corrections which can be comprehended as a high difference in localization via EKF on Trilateration location data and EKF on GNSS. The irrelevant generated location data of the trilateration method should be eliminated by a proper method. According to the results in Table 7, the maximum difference between EKF on Trilateration location data and

EKF on GNSS data in both environments is more than 7 meters and the average difference in the outdoor environment is almost 1 meter; therefore, it is obvious that Solvability method is not the proper validation method.

The trilateration location data validation method in the third and fourth rows of Table 7 is TimeStamp method. The third row contains the results of the localization within the hall and outdoor while the fourth row presents only the results of the experiment on the outdoor environment. Based on the third row, the result of the localization by EKF on the range data is more accurate than localization by EKF on the Trilateration location data. Figure 26 presents the comparison among entire methods and Figure 27 reveals the continuous localization of the Body frame via EKF on range data (red dots) and EKF on GNSS (green dots) in outdoor and within the hall. The jump value in the switching moment from GNSS to UWB localization is $9.29\ cm$ which is an adequate value in the case of wheel loader while this value for EKF on Trilateration location data is almost $51\ cm$. The average differences between localization via EKF on range data, EKF on Trilateration location data and EKF on GNSS are $4.60\ cm$ and $12.04\ cm$ and the maximum differences are $28.57\ cm$ and $63.86\ cm$, respectively. Referring to such results, the EKF on range data is more accurate than EKF on Trilateration location data.

In the case of the fourth row of Table 7, evidently, there is a more accurate localization via EKF on range data in comparison to EKF on Trilateration location data due to the characteristic of the Trilateration method which is not supposed to be implemented in the mobile cases. Figure 28 demonstrates the comparison of different methods of localization. Furthermore, owing to the environment of the experiment, localization is totally surveying on the GNSS data. The average differences via EKF on range data and EKF on Trilateration location data with EKF on GNSS data are $13.20\ cm$ and $37.21\ cm$, respectively.

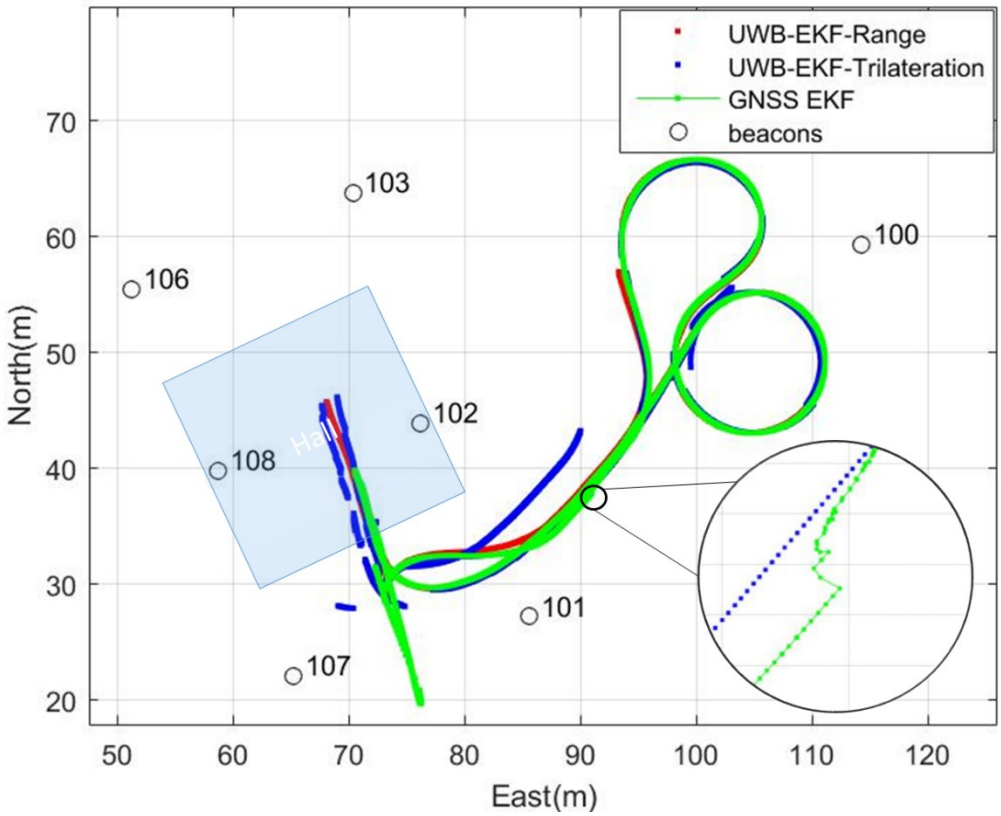

Figure 23. *Comparison of the Body origin location via EKF on range data, EKF on Trilateration location data by Solvability validation method and EKF on GNSS data within the Hall and outdoor*

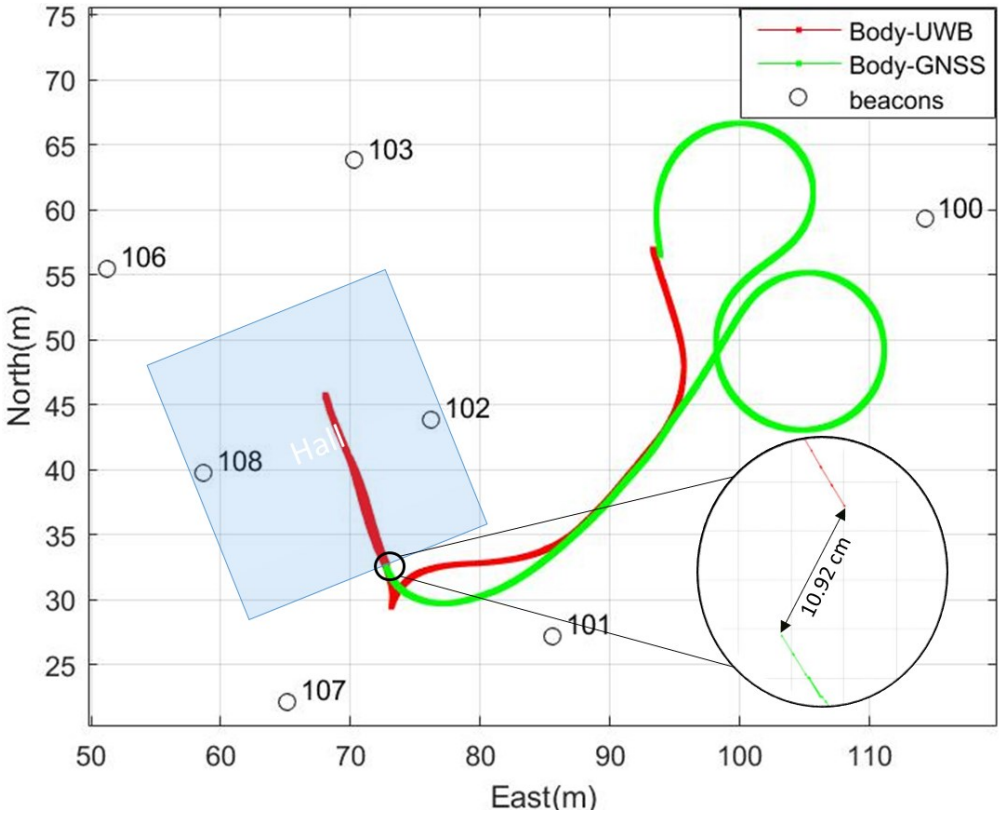

Figure 24. *Body origin Location via EKF GNSS and EKF on Range data by Solvability validation method in within the Hall and outdoor and jump point between GNSS and UWB*

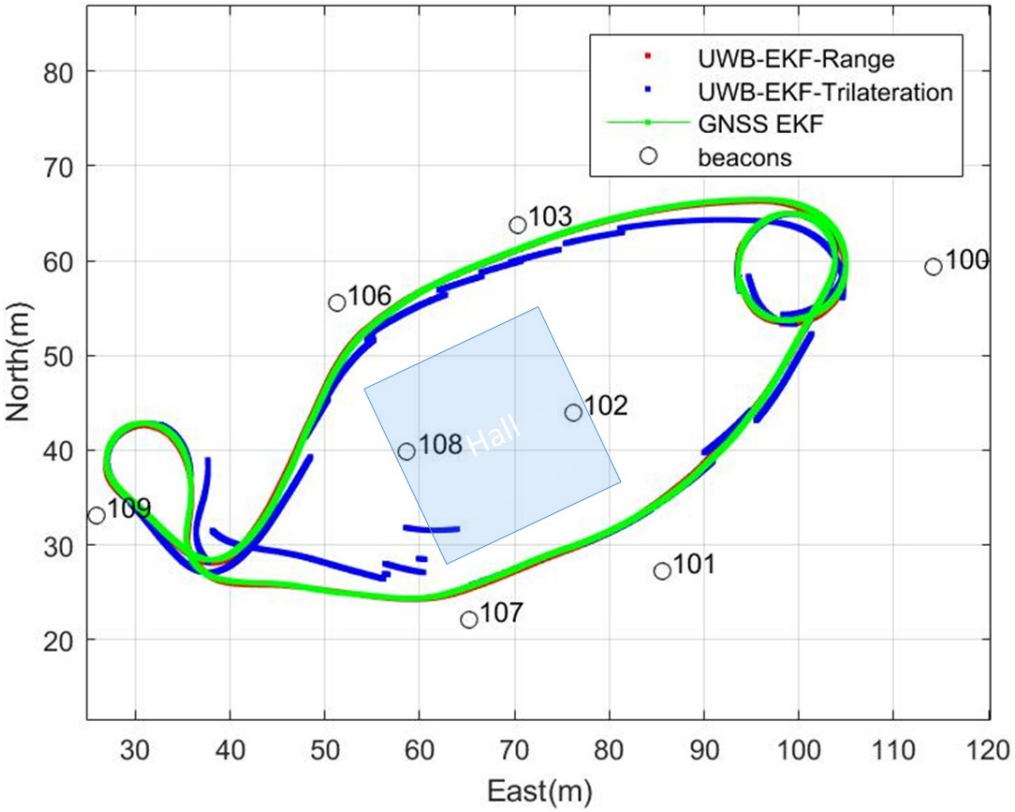

Figure 25. *Comparison of the Body origin location via EKF on range data, EKF on Trilateration location data by Solvability validation method and EKF on GNSS data in outdoor*

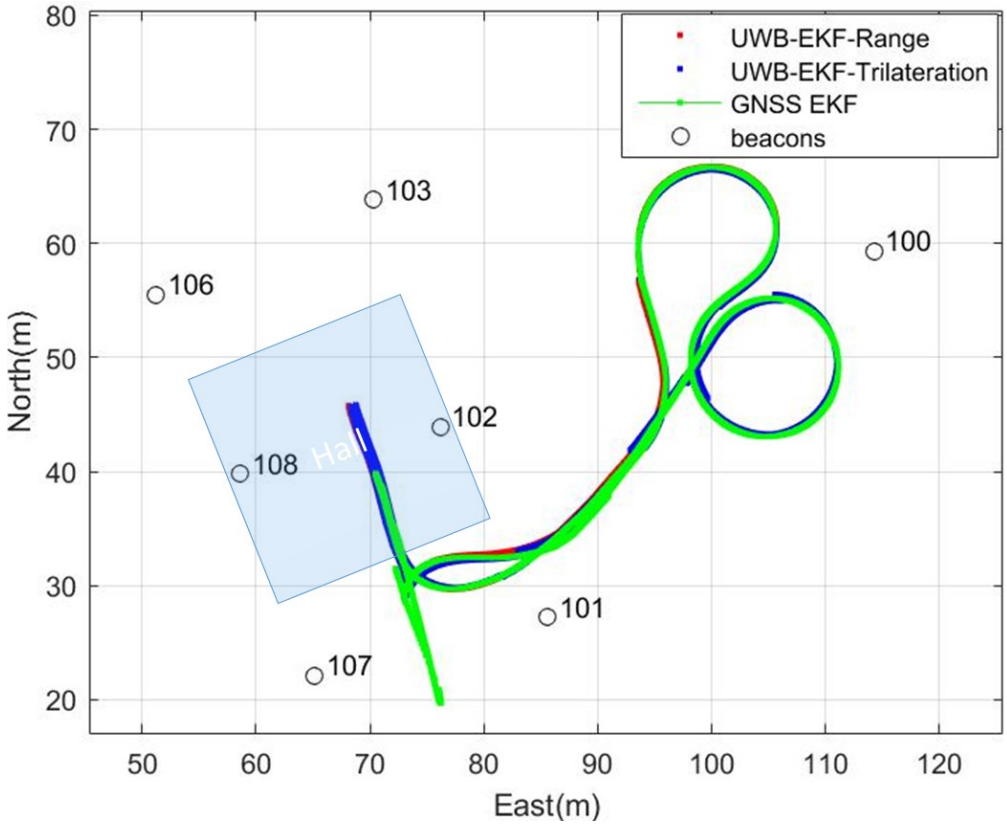

Figure 26. *Comparison of Body localization via EKF on range data, EKF on Trilateration location data by TimeStamp validation method and EKF on GNSS data within the Hall and outdoor*

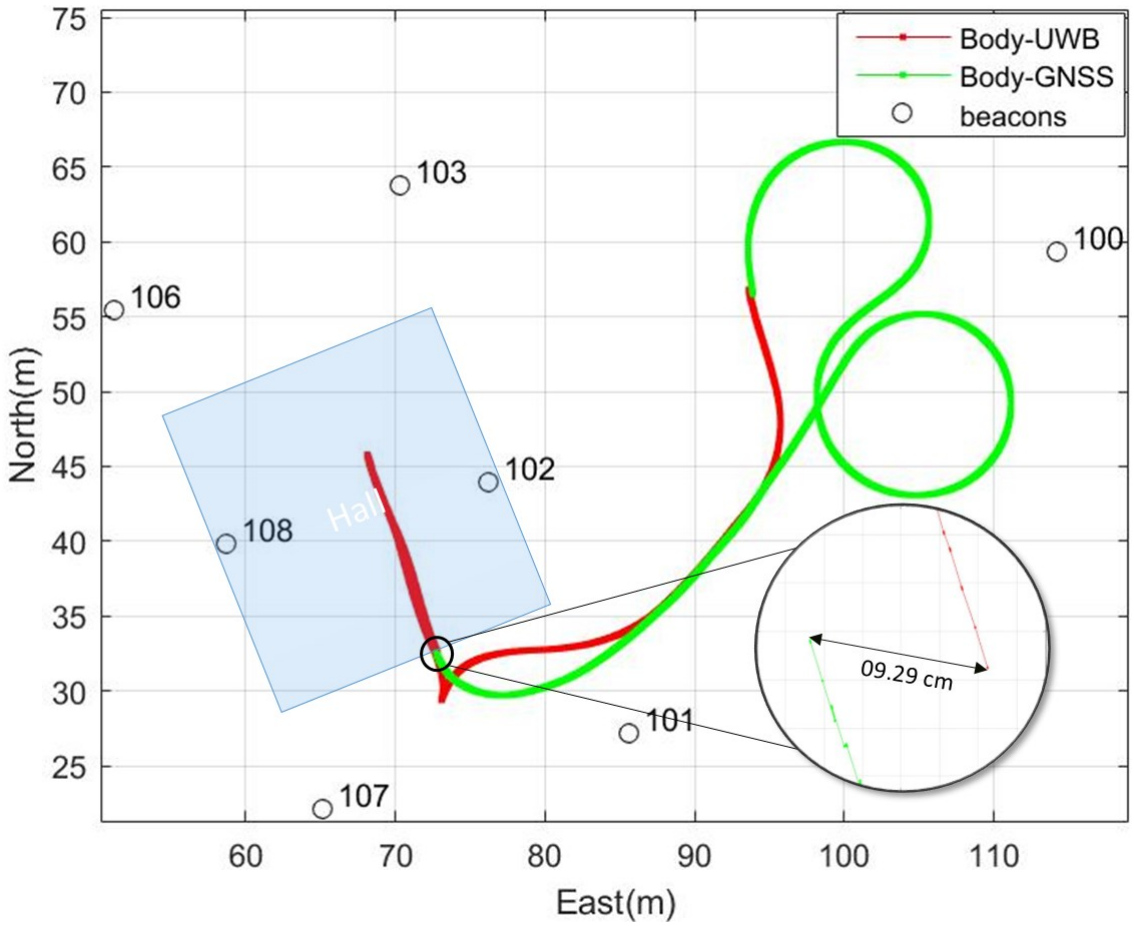

Figure 27. *Body origin Location via EKF GNSS and EKF on Range data via TimeStamp validation method within the Hall and outdoor*

The fifth row of Table 7 shows the results of the localization by Range Examination validation method within the hall and outdoor environment. In this case, localization on the EKF on range data is more accurate than on the EKF on Trilateration location data. Figure 29 illustrates the comparison of the localization method and Figure 30 presents the Body frame localization. The jump value in the switching moment from EKF on GNSS to EKF on range data localization is $5.41\ cm$ which can be seen in Figure 30 while this value in EKF on Trilateration location data localization is almost $52\ cm$. In the case of both average and maximum differences and also jump point value, the EKF on the range data has a better situation than EKF on Trilateration location data. The accuracy of EKF on range data and EKF on Trilateration location data are $6.32\ cm$ and $20.06\ cm$, accordingly.

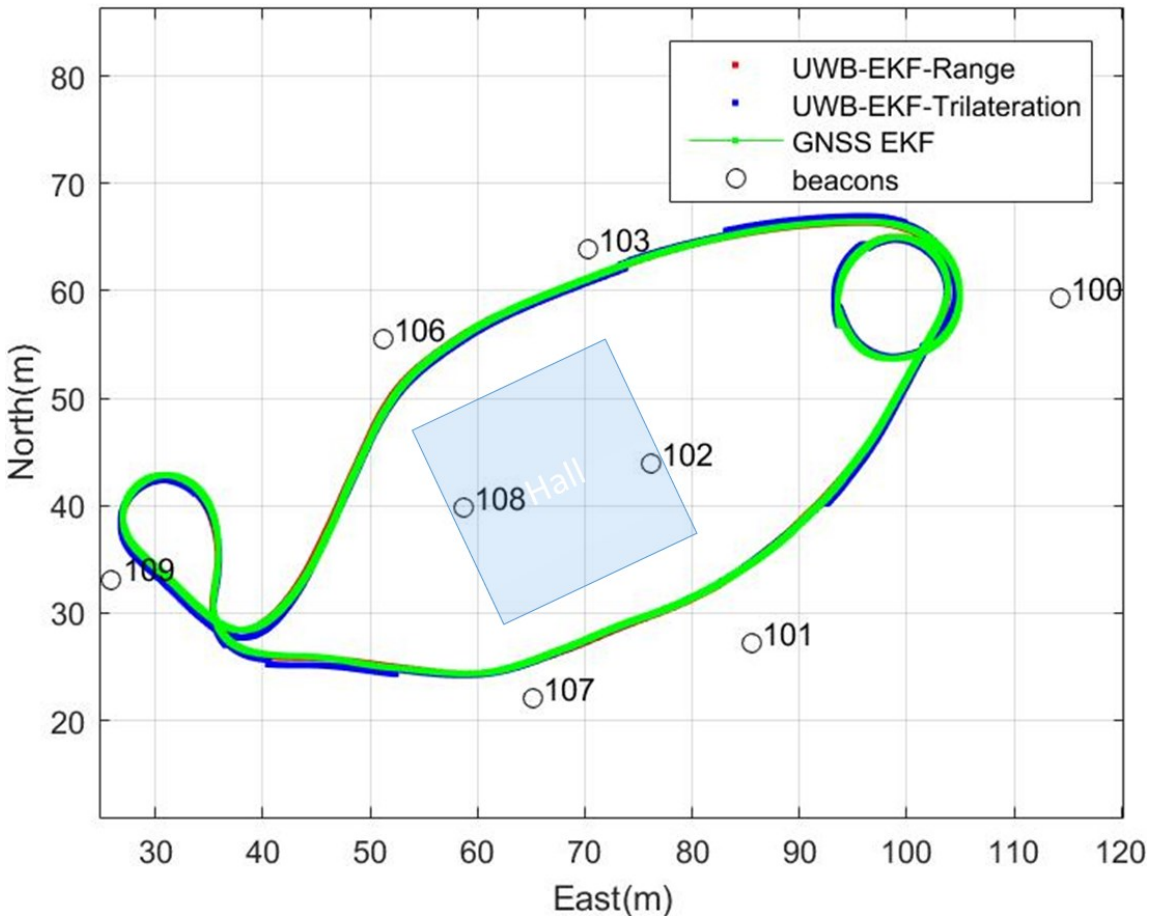

Figure 28. *Comparison of Body localization via EKF on range data, EKF on Trilateration location data by TimeStamp validation method and EKF on GNSS data in outdoor*

The last row of Table 7 indicates the results of the localization by both EKF on range data and on Trilateration location data via Range Examination validation method. Evidently, the EKF on range data is more accurate than the EKF on Trilateration location data. In this case, on account of the Trilateration method characteristics and the type of the validation method, the maximum difference of the EKF on Trilateration on location data is much higher than EKF on range data. Figure 31 illustrates the comparison of the localization methods and in this case, the final localization of the Body frame follows the GNSS data. The accuracy of EKF on range data and EKF on Trilateration location data are $19.72\ cm$ and $95.35\ cm$, respectively.

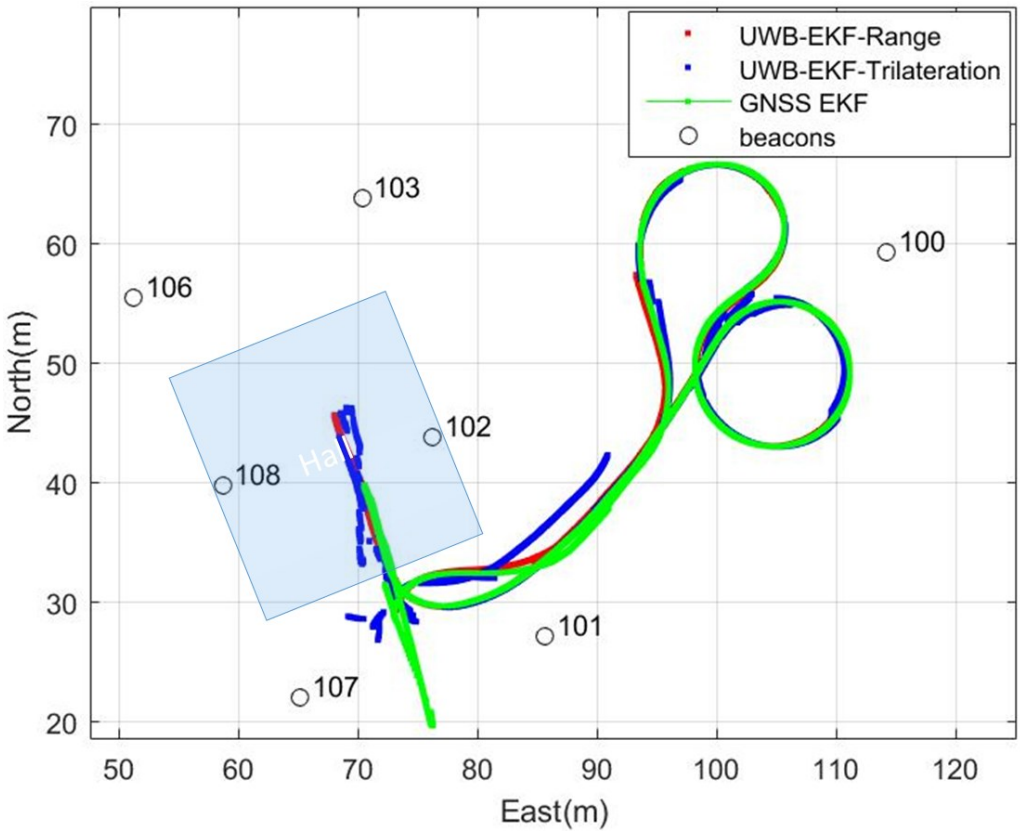

Figure 29. *Comparison of Body localization via EKF on range data and EKF on Trilateration location data by Range Examination validation method within the Hall and outdoor*

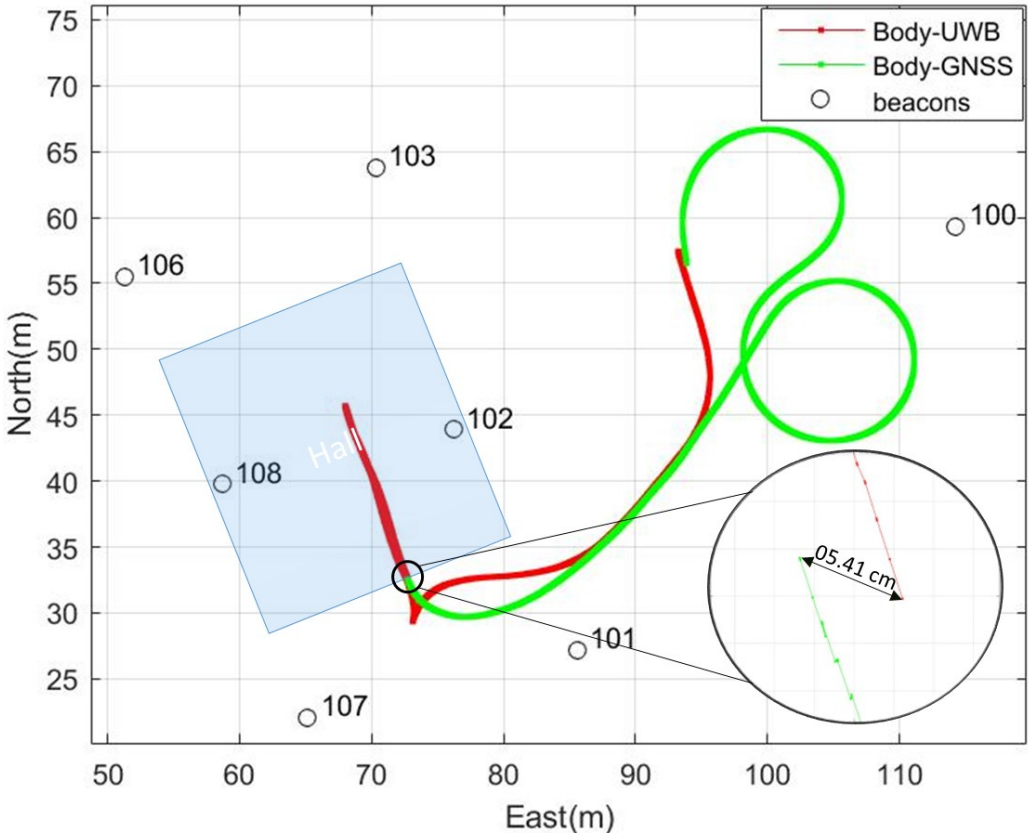

Figure 30. *Body localization via EKF GNSS and EKF on range data by Range Examination validation method within the Hall and outdoor*

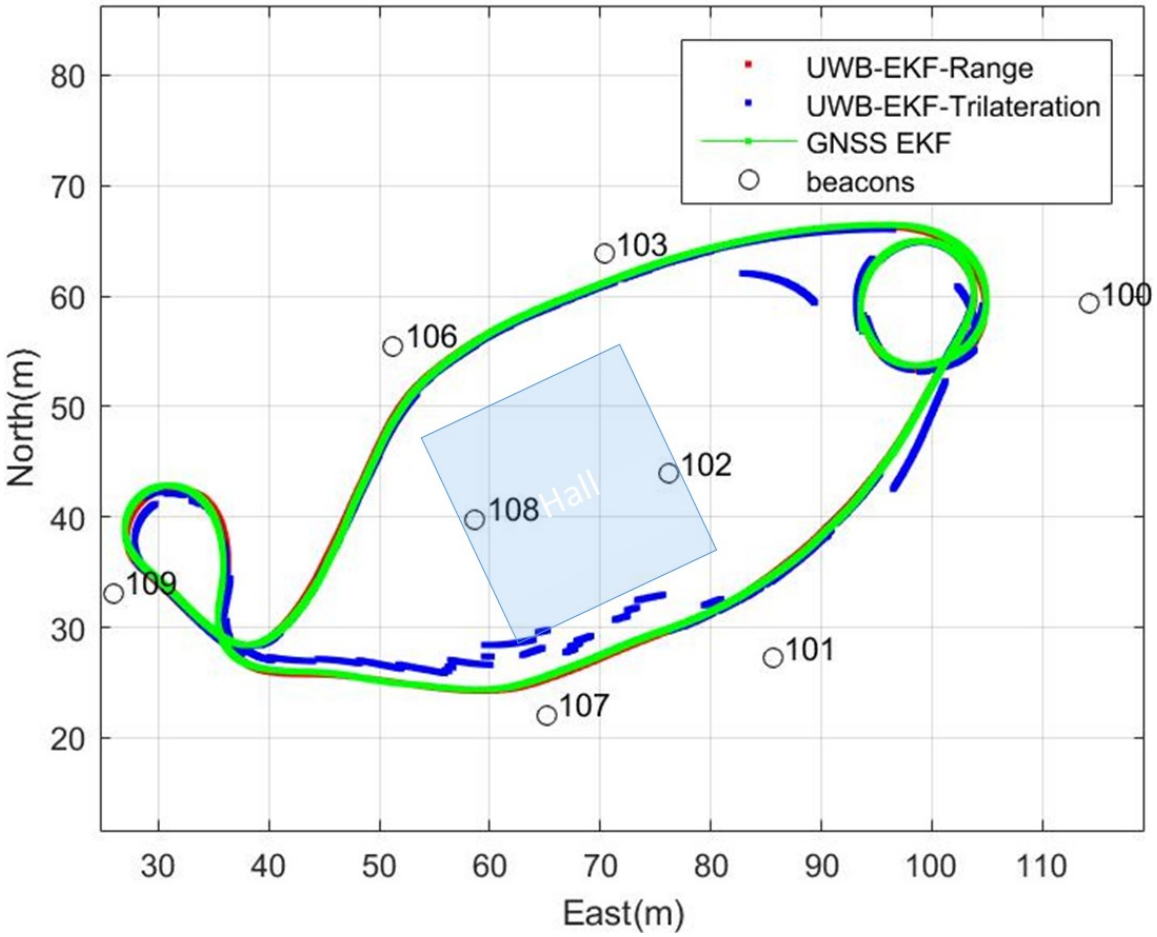

Figure 31. *Comparison of Body localization via EKF on range data and EKF on Trilateration location data with Range Examination validation method in outdoor*

4.8 Environment Analysis

This subchapter is dedicated to a short discussion regarding the effects of the experiment environment on the results. Figure 32, 33 and 34 indicate the results of the employing Solvability, Time Stamp and Range Examination validation data on the outdoor localization with trilateration method and the location data is in the UWB frame. Noticeably, the number of the undesired location data in the mentioned figures is less than Figures 19, 20 and 21 and the reason is less NLOS and reflected measurement signals due to the open space. However, when the wheel loader passes beside the Hall, more undesired location data appear in the Solvability and Range Examination methods. However, in the case of TimeStamp validation method, Figure 20 and 33, indicate that the number of the validated location data in the outdoor experiment is higher than the indoor and outdoor experiment and totally there is no undesired point. Yet there is another cause for the decline of the accuracy in the outdoor environment as the

results are expressed in Table 7 and that is variation in the height of the ground (z-axis) in some parts of the test area in the outdoor experiment. Near the anchor 109, the height of the ground is higher than the rest of the test area and in the algorithm of EKF on range data the value of z_t is imported from trilateration function block and due to that, it is not as accurate as the indoor and outdoor localization experiment because of the trilateration intrinsic error. As figure 20 presents, since the wheel loader is in the middle of the Hall, Owing to the high number of NLOS range measurement between mobile and anchor nodes which led to the incorrect location data, consequently, TimeStamp validation method ignores inaccurate generated location data, thus there is no location data from trilateration method, until it leaves the Hall. Meanwhile, the localization by EKF on Trilateration location data just follows the prediction. While there are no validated trilateration location data, the EKF on range data uses the last validated z_t value and LOS range measurements. Additionally, there is no drop in the accuracy because of no changing in the height of the wheel loader within the Hall. However, if there were proper roll and pitch, having more accurate localization was possible even by diverse ground height during the experiments.

Totally, localization could be highly affected by the environment if the localization method is only based on the geometric method such as Trilateration or Least Square Estimation methods which at least require having 3 range measurements from different anchors in a reasonable time duration and if one of the measurements among a set of measurements is not valid, it could be led to wrong location estimation and rejection from the validation method. While if the localization is based on the probabilistic methods such as Extended Kalman Filter, the localization would be influenced less than geometric methods by environment because even if there is no new validated range measurement or location data, the localization could be survived by prediction step which is employing angular velocities and direction velocities to predict the new location. Closed spaces could cause less accurate localization due to the growth in the number of NLOS range measurements while in our case because of the almost flat ground in the indoor environment there is no loss in the accuracy of EKF on range while accuracy of EKF on Trilateration location data is not as satisfying as the EKF on range data.

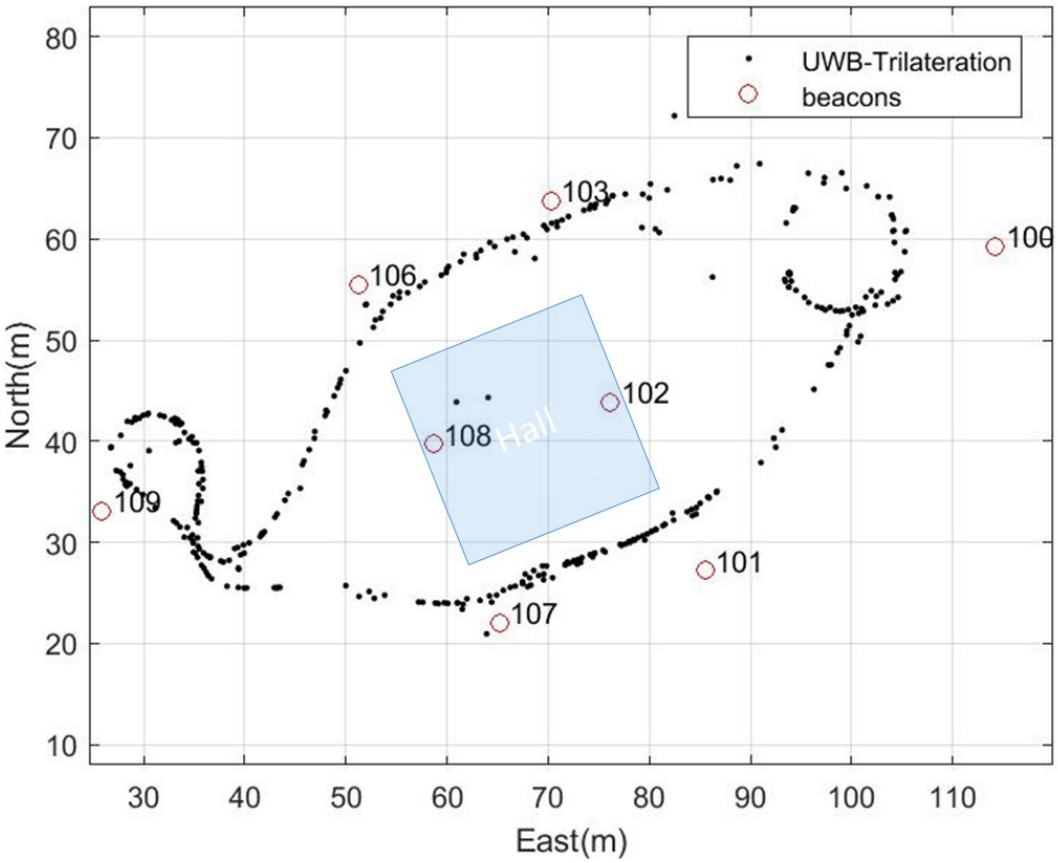

Figure 32. *Trilateration location data in UWB frame validated via Solvability method*

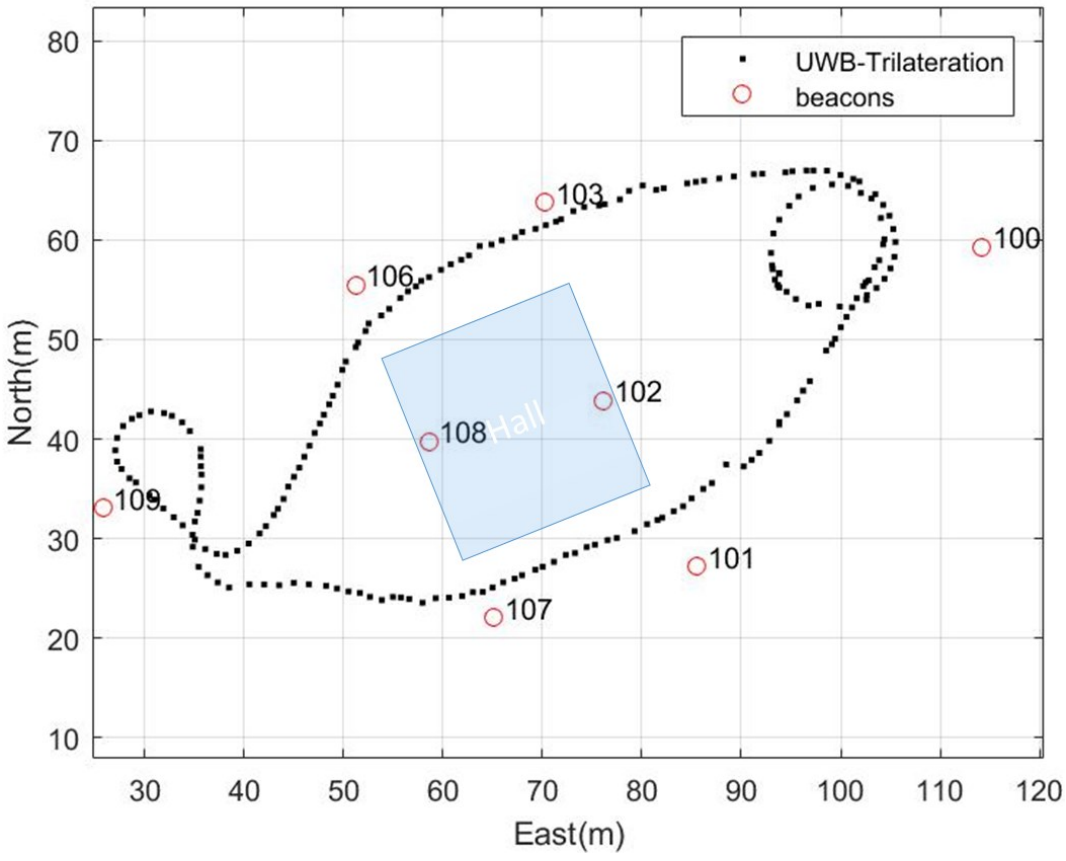

Figure 33. *Trilateration location data in UWB frame validated by Time Stamp method*

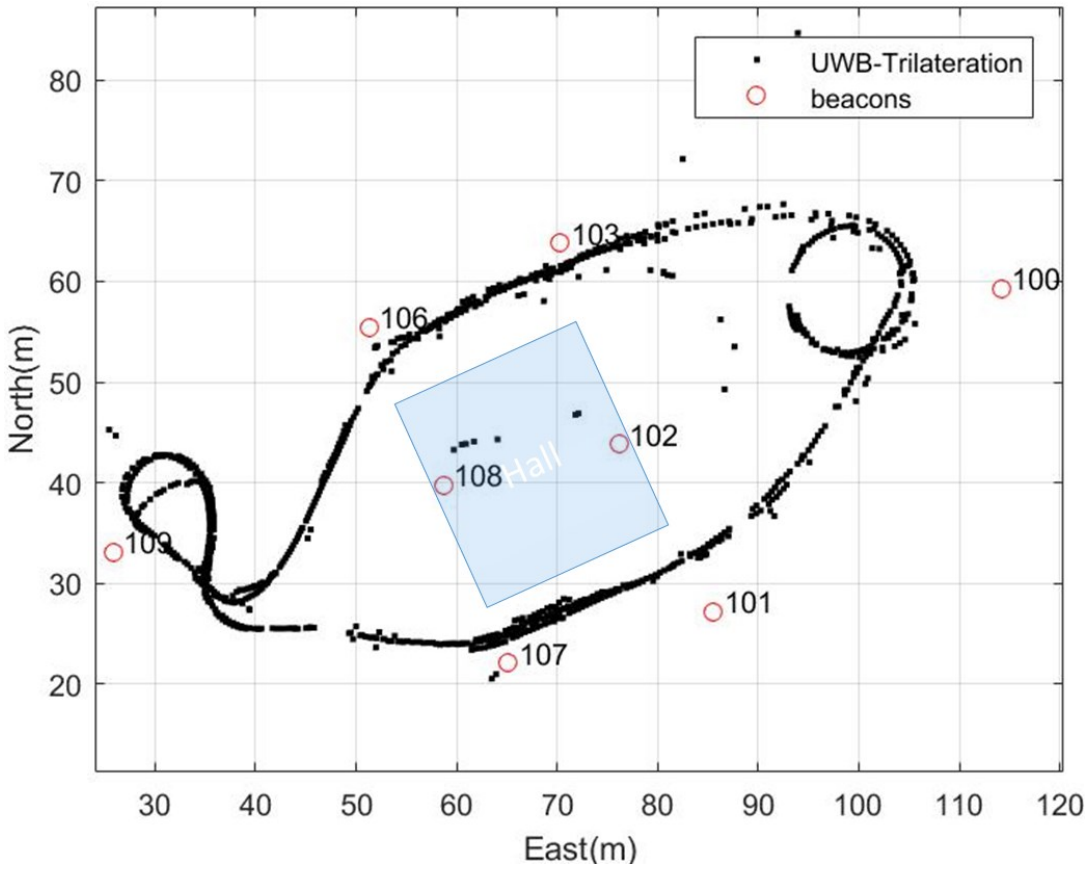

Figure 34. *Trilateration location data in UWB frame validated via Range Examination method*

5. CONCLUSION

Based on the experiments conducted, the EKF on the range data is more accurate than the EKF on the Trilateration location data. Totally, if there were a proper roll and pitch, it is possible to predict the z_t. Thus the correction factor in the EKF on range data which is $(z_n - \hat{z}_n)$ would present a higher performance. Consequently, the localization would be more accurate. The EKF on the Trilateration location data is not affected by this problem because it is not dependent on the z_t, while it suffers from substantial inaccuracy of the trilateration and the validation methods. Moreover, the inaccuracy has other reasons such as calibration of the UWB mobile node which was done by using a simple measuring tape and its accuracy is about a few millimeters and during the localization this few millimeters intensively affects the accuracy. The same situation is for calibration of the anchor nodes. By eliminating or debilitating these factors, having a more accurate localization with higher precision is possible.

According to the results of the experiments, the most comprehensive method to implement a localization with higher accuracy via UWB as a complementary localization of the GNSS will be achieved through estimation of the first position by employing the trilateration method and applying Range Examination validation method, due to its characteristics which has the best performance in the static situations. Plus, initialization of the yaw of the Extended Kalman Filter should be according to the yaw of the GNSS and then tracking the location by employing Extended Kalman Filter on the range data. In pursuance of having the best accuracy via this method, employing a proper IMU is necessary since the range measurement is in a 3-Dimensionals environment and in order to predict the measurement, having the prediction of the all axes are required. Replacing the prediction of the movement in any axis by other methods such as what is done in this research will be led to growing inaccuracy.

REFERENCES

[1] D. R. Brown and D. B. Dunn, “Classification schemes of positioning technologies for indoor navigation,” in *2011 Proceedings of IEEE Southeastcon*, 2011, pp. 125–130.

[2] O. Modest MANU, “A Study of Indoor Localization Techniques,” *DOCT-US Dr. Burses USV*, vol. 1, no. 2, p. 32, 2009.

[3] M. Uradzinski, H. Guo, X. Liu, and M. Yu, “Advanced Indoor Positioning Using Zigbee Wireless Technology,” *Wirel. Pers. Commun.*, vol. 97, no. 4, pp. 6509–6518, Dec. 2017.

[4] A. V. Juan Chóliz , Miguel Eguizábal , Ángela Hernández-Solana, “Comparison of Algorithms for UWB Indoor Location and Tracking Systems,” *IEEE Veh. Technol. Conf.*, pp. 1–5, 2011.

[5] “localization | Definition of localization in English by Oxford Dictionaries.” [Online]. Available: https://en.oxforddictionaries.com/definition/localization. [Accessed: 11-Sep-2018].

[6] S. Thrun, W. Burgard, and D. Fox, *Probabilistic robotics*. MIT Press, 2005.

[7] “GNSS / GPS Technology Differences | TerrisGPS.” [Online]. Available: http://www.terrisgps.com/gnss-gps-differences-explained/. [Accessed: 12-Sep-2018].

[8] J. Wang, T. Tsujii, C. Rizos, L. Dai, and M. Moore, “GPS AND PSEUDO-SATELLITES INTEGRATION FOR PRECISE POSITIONING.”

[9] V. Cantón Paterna, A. Calveras Augé, J. Paradells Aspas, and M. A. Pérez Bullones, “A Bluetooth Low Energy Indoor Positioning System with Channel Diversity, Weighted Trilateration and Kalman Filtering.,” *Sensors (Basel).*, vol. 17, no. 12, Dec. 2017.

[10] A. Alarifi *et al.*, “Ultra Wideband Indoor Positioning Technologies: Analysis and Recent Advances,” *Sensors*, vol. 16, no. 5, p. 707, 2016.

[11] Z. Farid, R. Nordin, and M. Ismail, “Recent advances in wireless indoor localization techniques and system,” *J. Comput. Networks Commun.*, vol. 2013, 2013.

[12] S. Gezici *et al.*, “Localization via Ultra-Wideband Radios [A look at positioning aspects of future sensor networks],” *IEEE Signal Process. Mag.*, 2005.

[13] S. Ullah, M. Ali, M. Asdaque Hussain, and K. Sup Kwak, “Applications of UWB Technology.”

[14] F. Dwiyasa and M.-H. Lim, “A survey of problems and approaches in wireless-based indoor positioning,” in *2016 International Conference on Indoor Positioning and Indoor Navigation (IPIN)*, 2016, pp. 1–7.

[15] R. Kshetrimayum, “An introduction to UWB communication systems,” *IEEE*

Potentials, vol. 28, no. 2, pp. 9–13, Mar. 2009.

[16] C. Laoudias, A. Moreira, S. Kim, S. Lee, L. Wirola, and C. Fischione, “A Survey of Enabling Technologies for Network Localization, Tracking, and Navigation,” *IEEE Commun. Surv. Tutorials*, no. July, 2018.

[17] M. Utter, “Indoor Positioning using Ultra-wideband Technology,” no. December, 2015.

[18] Y. Jiang and V. C. M. Leung, “An Asymmetric Double Sided Two-Way Ranging for Crystal Offset,” in *2007 International Symposium on Signals, Systems and Electronics*, 2007, pp. 525–528.

[19] IEEE, “IEEE 802.15.4a,” *IEEE Computer Society*, 2007. [Online]. Available: https://ieeexplore.ieee.org/stamp/stamp.jsp?arnumber=4299496. [Accessed: 03-Mar-2019].

[20] R. J. Fontana, “Recent System Applications of Short-Pulse Ultra-Wideband (UWB) Technology,” *IEEE Trans. Microw. Theory Tech.*, vol. 52, no. 9, pp. 2087–2104, Sep. 2004.

[21] K. Siwiak and D. Mc.Keown, “Ultra-Wideband Radio Technology,” 2004.

[22] Y. Rahayu, T. A. Rahman, R. Ngah, and P. S. Hall, “Ultra wideband technology and its applications,” in *2008 5th IFIP International Conference on Wireless and Optical Communications Networks (WOCN ’08)*, 2008, pp. 1–5.

[23] R. M. Kamins, R. E. Potter, and University of Hawaii (System), *Mālamalama : a history of the University of Hawai’i*. University of Hawai’i Press, 1998.

[24] X. S. Shen, W. Zhuang, H. Jiang, and J. Cai, “Medium Access Control in Ultra-Wideband Wireless Networks,” *IEEE Trans. Veh. Technol.*, vol. 54, no. 5, pp. 1663–1677, Sep. 2005.

[25] N. Abramson, “THE ALOHA SYSTEM-Another alternative for computer communications*.”

[26] L. G. Roberts and L. G., “ALOHA packet system with and without slots and capture,” *ACM SIGCOMM Comput. Commun. Rev.*, vol. 5, no. 2, pp. 28–42, Apr. 1975.

[27] M.-G. Di Benedetto, L. De Nardis, G. Giancola, and D. Domenicali, “The Aloha access (UWB)2 protocol revisited for IEEE 802.15.4a,” *ST J. Res.*, vol. 4, pp. 131–141, 2006.

[28] G. Miao, J. Zander, K. W. Sung, and S. Ben Slimane, *Fundamentals of Mobile Data Networks*. Cambridge: Cambridge University Press, 2016.

[29] E. H. Dinan and B. Jabbari, “Spreading codes for direct sequence CDMA and wideband CDMA cellular networks,” *IEEE Commun. Mag.*, vol. 36, no. 9, pp. 48–54, 1998.

[30] G. of R. Giunta, “Basic note on Spread Spectrum CDMA signals,” 2000.

[31] J. Li, X. Yue, J. Chen, and F. Deng, “A Novel Robust Trilateration Method Applied to Ultra-Wide Bandwidth Location Systems,” *Sensors*, vol. 17, no. 4, p. 795, Apr.

2017.

[32] V. Filonenko, “Asynchronous Ultrasonic Trilateration for Indoor Positioning of Mobile Phones.”

[33] S. Hu and T. Bao, “Ranging Optimization and Research on Indoor 3D Positioning Algorithm Based on UWB,” *J. Phys. Conf. Ser.*, vol. 1069, no. 1, 2018.

[34] A. Norrdine, “An Algebraic Solution to the Multilateration Problem,” *Proc. 15th Int. Conf. Indoor Position. Indoor Navig. Sydney, Aust.*, no. November 2012, pp. 3–6, 2012.

[35] M. I. Ribeiro, “Kalman and Extended Kalman Filters: Concept, Derivation and Properties,” 2004.

[36] M. S. Grewal and A. P. Andrews, *Kalman Filtering Theory and Practice Using MATLAB*. John Wiley & Sons, 2011.

[37] D. Simon, *Optimal State Estimation: Kalman, H∞, and Nonlinear Approaches*. John Wiley & Sons, Inc., 2006.

[38] T. Domain, “Data Sheet / User Guide,” no. July, pp. 1–46, 2015.

[39] T. Domain, “Data Sheet / User Guide,” no. July, pp. 1–46, 2015.

[40] “J1939-standard CANbus Solutions,” *Innodisk Corp.*, pp. 1–7, 2017.

[41] “SAE J1939 Standards Collection.” [Online]. Available: https://www.sae.org/standardsdev/groundvehicle/j1939a.htm. [Accessed: 10-Mar-2019].

[42] T. Domain, “RangeNet Application Programming Interface (API) Specificatio n,” pp. 1–156, 2017.

[43] Y. Zhang and F. Xi’An, “Multiplication-Based Pulse Integration for Detecting Underwater Target in Impulsive Noise Environment,” *IEEE Access*, vol. 4, pp. 6894–6900, 2016.

[44] B. Dewberry, “PulsON ® RangeNet / ALOHA Guide to Optimal Performance,” no. November, 2013.

[45] T. Domain, “RangeNet User Guide,” no. September, pp. 1–132, 2017.

[46] I. S. Ishak and R. Alinda Alias, “DESIGNING A STRATEGIC INFORMATION SYSTEMS PLANNING METHODOLOGY DESIGNING A STRATEGIC INFORMATION SYSTEMS PLANNING METHODOLOGY FOR MALAYSIAN INSTITUTES OF HIGHER,” no. May 2014, 2005.

[47] P. Szlávi and L. Zsakó, “IT competences: Modelling the real world,” *Ann. Math. Informaticae*, vol. 43, no. December 2014, pp. 183–199, 2014.

[48] MathWorks, “What is MATLAB?” [Online]. Available: https://se.mathworks.com/discovery/what-is-matlab.html.

[49] Python.org, “What is Python?”

[50] MathWorks, “Simulink real-time.”

[51] A. Norrdine, “An Algebraic Solution to the Multilateration Problem,” *2012 Int. Conf. Indoor Position. Indoor Navig.*, no. April, p. 2012, 2012.